A MESHLESS LOCAL BOUNDARY INTEGRAL EQUATION METHOD FOR HEAT CONDUCTION ANALYSIS IN NONHOMOGENEOUS SOLIDS

Jan Sladek*, Vladimir Sladek, and Chuanzeng Zhang

ABSTRACT

A local boundary integral equation method (LBIEM) with meshless approximation for heat conduction analysis in non-homogeneous solids is presented. A review of recent developments in advanced meshless LBIEM for 2-d, 3-d axisymmetric problems and microwave heating analysis is given. Both stationary and transient heat conduction problems are investigated in the paper. For transient problems both the Laplace transform technique and the time difference approach are applied to obtain the integral formulations using stationary or static fundamental solutions. Microwave heating is modelled by the forced heat equation with an exponential decay of the heat source intensity from an incident boundary. The thermal material properties are considered to be dependent on spatial coordinates. A pure boundary integral formulation is restricted to non-homogeneous solids with a special material gradation, where fundamental solutions can be obtained. To remove this restriction, an LBIEM is proposed to analyse the temperature distribution in general non-homogeneous solids. The moving least square (MLS) method is used for approximating the physical quantities in the local boundary integral equations (LBIEs). Numerical examples are given to demonstrate the high accuracy and efficiency of the implemented meshless LBIEM.

Key Words: meshless local boundary integral equation method, 2-d and 3-d axisymmetric heat conduction problems, microwave heating analysis, Laplace transform, time difference approach, MLS approximation, non-homogeneous solids.

I. INTRODUCTION

Functionally graded materials (FGMs) are non-homogeneous materials, and the volume fractions of their composite constituents are varying continuously in space. FGMs are preferred and favoured in many engineering structures and components due to their excellent thermal and mechanical properties (Miyamoto *et al.*, 1999; Suresh and Mortensen, 1998). Solution of boundary or initial boundary value problems for FGMs requires especially accurate and efficient numerical methods due to the high mathematical complexity caused by the material non-homogeneity. The finite element method (FEM), for the modelling of complex problems in applied mechanics and related fields, is well established. It is a robust and thoroughly developed technique, but it is not without its own shortcomings. It is well-known that the FEM relies on a mesh discretization, which leads to complications for certain classes of problems. Loss of accuracy is observed when the elements in the mesh become extremely skewed or distorted. The boundary element method (BEM) or boundary integral equation method (BIEM) has become an efficient and popular alternative to the FEM, especially for stress concentration and crack problems, or for boundary value problems wherein a part of the boundary extends to infinity. However, the pure BEM formulation can be applied only to cases where fundamental solutions are available. In many engineering

*Corresponding author. (Email: usarslad@savba.sk)

J. Sladek and V. Sladek are with the Insitute of Construction and Architecture, Slovak Academy of Science, 84503 Bratislava, Slovakia.

C. Zhang is with the Deparment of Civil Engineering, University of Applied Sciences Zittau/Görlitz, D-02763 Zittau.

applications, the fundamental solutions for the governing differential equations are either not available or they are too complex. Boundary value problems with continuously non-homogeneous material properties belong to this class. A remedy to overcome this difficulty is the application of the so-called boundary-domain integral formulation (Tanaka and Tanaka, 1980), in which only the fundamental solution for a homogeneous solid is required. In this case, the system matrix is fully populated including the nodal unknowns for the gradients of the primary physical quantities at interior nodes. For special cases such as exponentially graded materials, fundamental solutions or Green's functions have been derived by Martin *et al*. (2002), Gray *et al*. (2003), and Chan *et al*. (2003). A Laplace transform Galerkin boundary element method for transient heat conduction analysis in homogeneous and non-homogeneous materials has been presented by Sutradhar *et al*. (2002). Isoparametric graded elements within the framework of FEM has been developed by Kim and Paulino (2002).

In spite of the successful developments in FEM and BEM there has been a growing interest in the so-called meshless or meshfree methods over the past decade. A number of meshless methods has been proposed so far including the smooth particle hydrodynamics (SPH) method (Monaghan, 1988; Vignjevic *et al*., 2001), the diffuse element method (DEM) (Nayroles *et al*., 1992), the element free Galerkin (EFG) method (Belytschko *et al*., 1994; Gu and Liu, 2001a), the reproducing kernel particle method (RKPM) (Liu *et al*., 1993; Chen *et al*., 1998), the moving least-squares reproducing kernel (MLSRK) method (Li and Liu, 1996; Liu *et al*., 1997), the partition of unity finite element method (PUFEM) (Melenk and Babuska, 1996; Babuska and Melenk, 1997), the hp-clouds method (Duarte and Oden, 1996), the finite point method (Onate *et al*., 1996; Liu and Gu, 2001), the meshless local Petrov-Galerkin (MLPG) method (Atluri and Zhu, 1998; Liu and Atluri, 2000; Gu and Liu, 2001b; Ching and Batra, 2001), boundary node method (BNM) (Mukherjee and Mukherjee, 1997; Chati and Mukherjee, 2000), the local boundary integral equation (LBIE) method (Zhu *et al*., 1998; Atluri *et al*., 2000; Sladek *et al*., 2000a, 2000b; Sladek and Sladek, 2000; Sladek *et al*., 2001), and the method of finite spheres, which is a special case of the MLPG method when the local sub-domains are chosen to be spheres in three-dimensional cases (3-d) (De and Bathe, 2000). It will be beyond the scope of this paper to give a detailed review of the above mentioned meshless methods. For interested readers we refer to the review article by Belytschko *et al*. (1996), and a recent monograph by Atluri and Shen (2002).

Meshless methods were originated from the finite difference method (FDM), FEM and BEM, but meshless methods can treat an irregular distribution of nodes and require no costly mesh generation. In addition, since meshless methods use a functional basis and allow an arbitrary placement of nodes, the primary physical quantities and their derivatives may be found directly where they are needed and with a generally higher accuracy than in FDM, FEM and BEM, in which differentiations and interpolations are required. The term "meshless" or "meshfree" stems from the ability of an approximation or interpolation scheme to be constructed entirely from a set of nodes. The automatic generation of good quality meshes required in the conventional domain-type computational methods may become cumbersome in many engineering applications. This difficulty is circumvented in the meshless methods.

Many meshless formulations use the moving least-square (MLS) approximation for the physical quantities. One of the problems with the MLS interpolants is that they lack in general the delta function property of the usual shape functions applied in FEM or BEM. This complicates the imposition of the essential boundary conditions in the EFG method. Improved formulations of the EFG allowing a direct imposition of the essential boundary conditions have been suggested by Kaljevic and Saigal (1997), Mukherjee and Mukherjee (1997), and Gavete *et al*. (2000).

Although considerable efforts have been made recently in the development of meshless methods, the currently available meshless methods are still computationally much less efficient than the well established conventional discretization procedures. The primary reason is that the meshless methods use non-polynomial shape functions and the required numerical integration is difficult to perform accurately. Some progress leading to improved accuracy of the numerical integration and a unified stability analysis of meshless methods with Eulerian and Lagrangian kernels has been reported by Dolbow and Belytschko (1999) and Belytschko *et al*. (2000). An enhanced reliability in meshless methods can be achieved by means of self-adaptive techniques leading to refinements of cells, node density, and regions of influence of the nodes (Chung and Belytschko, 1998; Chati *et al*., 2001). It is worth mentioning that the cells are used just for the numerical integration, and pose no restrictions on the shape or compatibility. This feature makes meshless methods especially suited for self-adaptive techniques.

In this paper, a meshless LBIEM is presented for stationary and transient heat conduction analysis in non-homogeneous solids. The LBIEM is applied to two-dimensional (2-d), three-dimensional (3-d)

axisymmetric problems and microwave heating analysis. In section II, the basic idea of the meshless LBIEM is explained for 2-d heat conduction problems. The analyzed domain is divided into many small subdomains with a simple geometry such as circles. Because of the small size of the subdomains, one could assume that the material parameters within each subdomain are constant, and the fundamental solution corresponding to a homogeneous solid can be used (Zhu *et al*., 1998; De and Bathe, 2000; Atluri and Zhu, 1998). On the boundary of the subdomains, the LBIEs are applied. To eliminate the time variable in the differential equation for transient heat conduction problems, we use two different methods, namely, the Laplace transform method and the time-difference approach. In the Laplace transform formulation (Rizzo and Shippy, 1970), a pure boundary integral formulation can be obtained for homogeneous solids, where fundamental solutions for 2-d and 3-d axisymmetric problems are available and they consist of Bessel functions of the second kind. Since no fundamental solutions are available for transient heat conduction problems with variable thermal conductivity and diffusivity coefficients in general cases, we use a parametrix or Levi function (Mikhailov, 2002) instead of the fundamental solution in Green's formulae. The parametrix correctly describes the main part of the fundamental solutions but it is not required to satisfy the original governing equation. In particular, we use the fundamental solution corresponding to the Poisson's equation as a parametrix, which results in a boundary-domain integral formulation. If the LBIEs are applied to small subdomains with a simple circular geometry, domain integrals do not bring any difficulties in the numerical implementation. The LBIEs contain unknowns not only at the boundary but also at internal nodes. Each node is surrounded by a small circle, which is the boundary of a subdomain. On the boundary of a subdomain corresponding to an internal node both the temperature and the heat flux are unknowns. If the parametrix is vanishing identically on the boundary of a subdomain the number of unknowns is reduced, since the integral containing the product of the heat flux and the parametrix disappears. Different ways can be used to obtain a convenient parametrix vanishing on the boundary of a circular subdomain. The method based on a companion solution (Zhu *et al*., 1998) is more frequently used than the method with cut-off functions (Mikhailov, 2002). However, the second method seems to be more universal for a wide class of boundary value problems. Applying the MLS approximation to the LBIE, a system of linear algebraic equations is obtained. Several quasi-static boundary value problems have to be solved for various discrete values of the Laplace transform parameter. Then, the time-dependent solutions can be obtained by the Stehfest inversion method (Stehfest, 1970). In the time-difference approach, the time variation of the temperature is approximated by a finite difference scheme, which converts the linear parabolic differential equation into a linear elliptic differential equation (Curran *et al*., 1980). Like in the Laplace transform method, a simple fundamental solution corresponding to the Poisson's equation is used to derive the LBIEs. The spatial variation of the temperature is approximated by the same meshless scheme applied in the Laplace transform method.

Section III is devoted to 3-d axisymmetric heat conduction problems. The axial symmetry of the geometry and boundary conditions for a 3-d solid reduces an initial-boundary value problem to a 2-d problem. The transient heat conduction problem for a homogeneous solid was investigated by Brebbia *et al*. (1984). The conventional boundary integral formulation in the time-difference approach requires a complex fundamental solution proportional to the modified Bessel function of the first kind. If the same fundamental solution is applied to a non-homogeneous solid, a boundary-domain integral formulation is obtained. In this case, the evaluation of domain integrals with the complex fundamental solution increases the computing time used for the numerical analysis. Moreover, the integral representation for the temperature gradients at interior points has to be added to obtain a unique integral formulation. It should be noted that the singularity of the kernel in the integral representation formula for the temperature gradients is increased to a hypersingularity. In this paper, we present an alternative way based on the meshless LBIEM, where the analyzed domain is divided into small subdomains with a simple circular geometry. The Laplace transform method is applied for eliminating the time dependence in the heat conduction equation, while the same meshless scheme is adopted for the spatial approximation of the LBIEs.

In section IV, a microwave heating analysis is performed by using the meshless LBIEM. In our analysis, microwave heating is analyzed as a 2-d diffusion problem with prescribed body heat sources and material non-homogeneity. The use of microwave heating has attracted much attention in industrial processes due to its high efficiency. A crucial point in microwave heating is to analyze hot spots, which are regions where temperature is quickly rising. This phenomenon is induced by the temperature dependence of the material properties, namely, the thermal absorptivity increases with increasing temperature. Hot spots out of control can damage the sample in an industrial process. The first attempt to analyze hot spots in a homogeneous solid was made by Zhu *et al*. (1995), who used a dual reciprocity boundary element

method (DRBEM). In the DRBEM, some interior nodes have to be supplemented to boundary nodes for an adequate spatial approximation of physical fields in transforming domain integrals into boundary integrals. In this paper, a local BIEM for microwave heating analysis in FGMs is presented. Since a pure boundary integral formulation for the global boundary requires the availability of the fundamental solutions for non-homogeneous solids which are yet not known, to our knowledge, we apply the meshless LBIEM by using a simple static fundamental solution corresponding to the Poisson's equation. The Laplace transform method is used for eliminating the time variable in the heat conduction equation. For the spatial approximation, the same meshless scheme as applied for 2-d and 3-d axisymmetric heat conduction analysis is adopted.

Numerical examples are given in the individual sections to demonstrate the accuracy and efficiency of the meshless LBIEM. Some conclusions are given in section V to summarize the essential features of the meshless LBIEM for heat conduction analysis in continuously non-homogeneous solids.

II. TRANSIENT HEAT CONDUCTION PROBLEM IN 2-D

1. Laplace Transform Formulation

Let us consider a boundary value problem for the heat conduction equation in two-dimensional cases, which is governed by

$$\theta_{,ii}(\boldsymbol{x},t) - \frac{1}{\kappa(\boldsymbol{x})}\frac{\partial\theta}{\partial t}(\boldsymbol{x},t) + \frac{k_{,i}}{k}(\boldsymbol{x})\theta_{,i}(\boldsymbol{x},t) = -\frac{Q}{\kappa(\boldsymbol{x})}(\boldsymbol{x},t) \tag{1}$$

where $\theta(\boldsymbol{x}, t)$ is the temperature field, $Q(\boldsymbol{x}, t)$ is the density of body heat sources, k and κ stand for the thermal conductivity and diffusivity, respectively. The material parameters are assumed to be continuously dependent on Cartesian coordinates.

Applying the Laplace transform to the governing Eq. (1) we obtain (Balas *et al*., 1989)

$$\overline{\theta}_{,ii}(\boldsymbol{x}, p) - \frac{p}{\kappa}\overline{\theta}(\boldsymbol{x}, p) + \frac{k_{,i}}{k}(\boldsymbol{x})\overline{\theta}_{,i}(\boldsymbol{x}, p) = -\frac{1}{\kappa}\overline{F}(\boldsymbol{x}, p) \tag{2}$$

where

$$\overline{F}(\boldsymbol{x}, p) = \overline{Q}(\boldsymbol{x}, p) + \theta(\boldsymbol{x}, 0)$$

is the modified body heat source in the Laplace transform domain including the initial boundary condition for the temperature field, and p is the Laplace transform parameter.

By applying the Gauss divergence theorem to the weak formulation of Eq. (2), we get an integral representation for the temperature field in the Laplace transform domain

$$\begin{aligned}\overline{\theta}(\boldsymbol{y}, p) &= \int_\Gamma \frac{\partial\overline{\theta}}{\partial n}(\boldsymbol{x}, p)\theta^*(\boldsymbol{x}, \boldsymbol{y})d\Gamma - \int_\Gamma \overline{\theta}(\boldsymbol{x}, p)\frac{\partial\theta^*}{\partial n}(\boldsymbol{x}, \boldsymbol{y})d\Gamma \\ &\quad - \int_\Omega \frac{p}{\kappa(\boldsymbol{x})}\overline{\theta}(\boldsymbol{x}, p)\theta^*(\boldsymbol{x}, \boldsymbol{y})d\Omega \\ &\quad + \int_\Omega \frac{k_{,i}}{k}(\boldsymbol{x})\overline{\theta}_{,i}(\boldsymbol{x}, p)\theta^*(\boldsymbol{x}, \boldsymbol{y})d\Omega \\ &\quad + \int_\Omega \frac{1}{\kappa(\boldsymbol{x})}\overline{F}(\boldsymbol{x}, p)\theta^*(\boldsymbol{x}, \boldsymbol{y})d\Omega \end{aligned} \tag{3}$$

where $\boldsymbol{y}\in\Omega$ and the fundamental solution $\theta^*(\boldsymbol{x}, \boldsymbol{y}) = -\frac{1}{2\pi}\ln r$ is the solution of the Poisson's equation .

$$\theta^*_{,ii}(\boldsymbol{x}, \boldsymbol{y}) + \delta(\boldsymbol{x}, \boldsymbol{y}) = 0 \tag{4}$$

In the fundamental solution r denotes the distance of field and collocation points, $r=|\boldsymbol{x}-\boldsymbol{y}|$. If the collocation point $\boldsymbol{y}$ is on the global boundary Γ ($\boldsymbol{y}\to\zeta\in\Gamma$), Eq. (4) becomes

$$\begin{aligned}&\int_\Gamma [\overline{\theta}(\boldsymbol{x}, p) - \overline{\theta}(\zeta, p)]\theta^*(\boldsymbol{x}, \zeta)d\Gamma \\ &\quad - \int_\Gamma \frac{\partial\overline{\theta}}{\partial n}(\boldsymbol{x}, p)\theta^*(\boldsymbol{x}, \zeta)d\Gamma \\ &= -\int_\Omega \frac{p}{\kappa(\boldsymbol{x})}\overline{\theta}(\boldsymbol{x}, p)\theta^*(\boldsymbol{x}, \zeta)d\Omega \\ &\quad + \int_\Omega \frac{k_{,i}}{k}(\boldsymbol{x})\overline{\theta}_{,i}(\boldsymbol{x}, p)\theta^*(\boldsymbol{x}, \zeta)d\Omega \\ &\quad + \int_\Omega \frac{1}{\kappa(\boldsymbol{x})}\overline{F}(\boldsymbol{x}, p)\theta^*(\boldsymbol{x}, \zeta)d\Omega \end{aligned} \tag{5}$$

The boundary integral Eq. (5) has to be supplemented by the integral representation of the temperature gradients at interior points, in order to derive a unique set of equations. Although the problem of singularities has been resolved successfully in such a formulation, the discretization of both the boundary and the interior domain is required. Consequently,

two sets of coupled algebraic equations, for boundary and interior unknowns, have to be solved.

Another approach is to use the boundary-domain formulation on simple circular domains around each of the (randomly) distributed nodal points within the analyzed domain. If, instead of the entire domain Ω, we consider a subdomain Ω_s, the following local boundary integral equation should also hold over the subdomain

$$\begin{aligned}\overline{\theta}(\mathbf{y}, p) = &\int_{\partial\Omega_s} \frac{\partial \overline{\theta}}{\partial n}(\mathbf{x}, p)\theta^*(\mathbf{x}, \mathbf{y})d\Gamma \\ &- \int_{\partial\Omega_s} \overline{\theta}(\mathbf{x}, p)\frac{\partial \theta^*}{\partial n}(\mathbf{x}, \mathbf{y})d\Gamma \\ &- \int_{\Omega_s} \frac{p}{\kappa(\mathbf{x})}\overline{\theta}(\mathbf{x}, p)\theta^*(\mathbf{x}, \mathbf{y})d\Omega \\ &+ \int_{\Omega_s} \frac{k_{,i}}{k}(\mathbf{x})\overline{\theta}_{,i}(\mathbf{x}, p)\theta^*(\mathbf{x}, \mathbf{y})d\Omega \\ &+ \int_{\Omega_s} \frac{1}{\kappa(\mathbf{x})}\overline{F}(\mathbf{x}, p)\theta^*(\mathbf{x}, \mathbf{y})d\Omega \end{aligned} \tag{6}$$

The integral Eq. (6) is considered for small subdomains $\Omega_s \subset \Omega$. Hence, none of the boundary densities in the Laplace transformed domain are prescribed on the local boundary $\partial\Omega_s$ as long as they lie entirely inside Ω. This deficit in boundary conditions inside the domain Ω is overcome by the domain type approximation of field variables. For such an approximation the boundary-domain formulation (6) doesn't bring any difficulties with the domain integral evaluation on a simple subdomain (Sladek *et al.*, 2000b). Namely, making use of domain-type approximation for $\overline{\theta}(\mathbf{x}, p)$, the expression for the approximation of $\partial\overline{\theta}/\partial n$ can be obtained by differentiating the primary field quantity $\overline{\theta}(\mathbf{x}, p)$. The accuracy of the approximation of temperature gradients or derivatives is lower than the one for primary field , i.e., temperature. Therefore, it is more convenient to reduce the number of unknowns on $\partial\Omega_s$ in each LBIE before introducing any approximation. Such a reduction is feasible from the freedom in the choice of the shape of $\partial\Omega_s$. For a circular subdomain the concept of a companion solution (Zhu *et al.*, 1998; Atluri *et al.*, 2000) can be employed. It is seen that

$$\tilde{\theta}^*(r) = \frac{1}{2\pi}\ln\frac{r_0}{r} \tag{7}$$

is the Green's function for the Possion's equation vanishing on the boundary of the circular subdomain of radius r_0.

Thus, $\tilde{\theta}^*$ can be used as a new test function. This leads to the following simplifications of the LBIE (6)

$$\begin{aligned}\overline{\theta}(\mathbf{y}, p) = &-\int_{\partial\Omega_s} \overline{\theta}(\mathbf{x}, p)\frac{\partial \tilde{\theta}^*}{\partial n}(\mathbf{x}, \mathbf{y})d\Gamma \\ &- \int_{\Omega_s} \frac{p}{\kappa(\mathbf{x})}\overline{\theta}(\mathbf{x}, p)\tilde{\theta}^*(\mathbf{x}, \mathbf{y})d\Omega \\ &+ \int_{\Omega_s} \frac{k_{,i}}{k}(\mathbf{x})\overline{\theta}_{,i}(\mathbf{x}, p)\tilde{\theta}^*(\mathbf{x}, \mathbf{y})d\Omega \\ &+ \int_{\Omega_s} \frac{1}{\kappa(\mathbf{x})}\overline{F}(\mathbf{x}, p)\tilde{\theta}^*(\mathbf{x}, \mathbf{y})d\Omega \end{aligned} \tag{8}$$

as long as $\mathbf{y} \in \Omega$. For $\mathbf{y} = \zeta \in \partial\Omega$, the LBIE (6) takes the following form

$$\begin{aligned}\overline{\theta}(\mathbf{y}, p) = &-\int_{L_s} \overline{\theta}(\mathbf{x}, p)\frac{\partial \tilde{\theta}^*}{\partial n}(\mathbf{x}, \zeta)d\Gamma \\ &- \lim_{y\to\zeta}\int_{\Gamma_s} \overline{\theta}(\mathbf{x}, p)\frac{\partial \tilde{\theta}^*}{\partial n}(\mathbf{x}, \mathbf{y})d\Gamma \\ &+ \int_{\Gamma_s} \frac{\partial \overline{\theta}}{\partial n}(\mathbf{x}, p)\tilde{\theta}^*(\mathbf{x}, \zeta)d\Gamma \\ &- \int_{\Omega_s} \frac{p}{\kappa(\mathbf{x})}\overline{\theta}(\mathbf{x}, p)\tilde{\theta}^*(\mathbf{x}, \zeta)d\Omega \\ &+ \int_{\Omega_s} \frac{k_{,i}}{k}(\mathbf{x})\overline{\theta}_{,i}(\mathbf{x}, p)\tilde{\theta}^*(\mathbf{x}, \zeta)d\Omega \\ &+ \int_{\Omega_s} \frac{1}{\kappa(\mathbf{x})}\overline{F}(\mathbf{x}, p)\tilde{\theta}^*(\mathbf{x}, \zeta)d\Omega \end{aligned} \tag{9}$$

where L_s is the circular part of $\partial\Omega_s$ and $\Gamma_s = \partial\Omega_s - L_s$, if the collocation point lies on the global boundary, i.e., $\mathbf{y} \in \partial\Omega$.

The Green's function $\tilde{\theta}^*$ is the parametrix for the transient heat conduction problem in a continuously nonhomogeneous solid since it satisfies only the main part of the governing Eq. (1). Now, we can apply another way to obtain the Green's function. We can choose a function (Mikhailov, 2002)

$$P^*(r) = \chi(r)\frac{1}{2\pi}\ln\frac{1}{r} \tag{10}$$

where $\chi(r)$ is a cut-off function, such that

$$\chi(r) = \begin{cases} 1 & r \neq r_0 \\ 0 & r = r_0 \end{cases} \tag{11}$$

The requirements in Eq. (11) are satisfied by the following function

$$\chi(r) = 1 - \frac{r^2}{r_0^2} \tag{12}$$

The LBIE with the parametrix $P^*(\boldsymbol{x}, \boldsymbol{y})$ has the following form

$$\begin{aligned}\overline{\theta}(\boldsymbol{y}, p) = &- \int_{\partial\Omega_s} \overline{\theta}(\boldsymbol{x}, p)\frac{\partial P^*}{\partial n}(\boldsymbol{x}, \boldsymbol{y})d\Gamma \\ &+ \int_{\Omega_s} \overline{\theta}(\boldsymbol{x}, p)[R(\boldsymbol{x}, \boldsymbol{y}) - \frac{p}{\kappa(\boldsymbol{x})}P^*(\boldsymbol{x}, \boldsymbol{y})]d\Omega \\ &+ \int_{\Omega_s} \frac{k_{,i}}{k}(\boldsymbol{x})\overline{\theta}_{,i}(\boldsymbol{x}, p)P^*(\boldsymbol{x}, \boldsymbol{y})d\Omega \\ &+ \int_{\Omega_s} \frac{1}{\kappa(\boldsymbol{x})}\overline{F}(\boldsymbol{x}, p)P^*(\boldsymbol{x}, \boldsymbol{y})d\Omega \end{aligned} \tag{13}$$

where

$$R(\boldsymbol{x}, \boldsymbol{y}) = \frac{2}{\pi r_0^2}(1 + \ln r) \tag{14}$$

Similarly one can write the LBIE at $\boldsymbol{y}=\zeta\in\partial\Omega$ as

$$\begin{aligned}&\overline{\theta}(\boldsymbol{y}, p) \\ &= - \int_{L_s} \overline{\theta}(\boldsymbol{x}, p)\frac{\partial P^*}{\partial n}(\boldsymbol{x}, \zeta)d\Gamma \\ &\quad - \lim_{y\to\zeta}\int_{\Gamma_s} \overline{\theta}(\boldsymbol{x}, p)\frac{\partial P^*}{\partial n}(\boldsymbol{x}, \boldsymbol{y})d\Gamma \\ &\quad + \int_{\Gamma_s} \frac{\partial\overline{\theta}}{\partial n}(\boldsymbol{x}, p)P^*(\boldsymbol{x}, \zeta)d\Gamma \\ &\quad + \int_{\Omega_s} \overline{\theta}(\boldsymbol{x}, p)[R(\boldsymbol{x}, \zeta) - \frac{p}{\kappa(\boldsymbol{x})}P^*(\boldsymbol{x}, \zeta)]d\Omega \\ &\quad + \int_{\Omega_s} \frac{k_{,i}}{k}(\boldsymbol{x})\overline{\theta}_{,i}(\boldsymbol{x}, p)P^*(\boldsymbol{x}, \zeta)d\Omega \\ &\quad + \int_{\Omega_s} \frac{1}{\kappa(\boldsymbol{x})}\overline{F}(\boldsymbol{x}, p)P^*(\boldsymbol{x}, \zeta)d\Omega \end{aligned} \tag{15}$$

The LBIEs (13) and (15) are the alternative LBIE formulation to the previous one given by Eqs. (8) and (9). The only difference lies in the used integral kernels. The method with a cut-off function seems to be more universal to construct a proper localized parametrix.

The moving least squares (MLS) method (Belytschko *et al*., 1994; Belytschko *et al*., 1996; Atluri *et al*., 1999) is considered as the domain-type approximation for the Laplace transformed field quantities either in the LBIEs (8) and (9) or in Eqs. (13) and (15). The approximated function can be written as

$$\overline{\theta}^h(\boldsymbol{x}, p) = \boldsymbol{\Phi}^T(\boldsymbol{x}) \cdot \hat{\theta}(p) = \sum_{a=1}^{n} \phi^a(\boldsymbol{x})\hat{\theta}^a(p) \tag{16}$$

where $\hat{\theta}^a$ is the fictitious nodal value and $\phi^a(\boldsymbol{x})$ is the shape function associated with the node a. The number of nodes n, used for the approximation of $\overline{\theta}(\boldsymbol{x}, p)$, is determined by the weight function $w^a(\boldsymbol{x})$. A Gaussian weight function is considered in the present analysis. The directional derivatives of $\overline{\theta}(\boldsymbol{x}, p)$ are approximated by the same nodal values as

$$\frac{\partial\overline{\theta}^h}{\partial n}(\boldsymbol{x}, p) = n_k(\boldsymbol{x})\sum_{a=1}^{n} \hat{\theta}^a(p)\phi^a_{,k}(\boldsymbol{x}) \tag{17}$$

Making use of the MLS-approximation (16) for $\overline{\theta}(\boldsymbol{x}, p)$, the LBIEs (8) and (9) yield the following set of equations:

$$\begin{aligned}&\sum_{a=1}^{n} \{\phi^a(\boldsymbol{y}^b) + \int_{\partial\Omega_s} \frac{\partial\tilde{\theta}^*}{\partial n}(\boldsymbol{x}, \boldsymbol{y}^b)\phi^a(\boldsymbol{x})d\Gamma\}\hat{\theta}^a(p) \\ &= - \sum_{a=1}^{n} \int_{\Omega_s} \tilde{\theta}^*(\boldsymbol{x}, \boldsymbol{y}^b)[\frac{p}{\kappa(\boldsymbol{x})}\phi^a(\boldsymbol{x}) - \frac{k_{,i}}{k}(\boldsymbol{x})\phi^a_{,i}(\boldsymbol{x})] \\ &\quad \cdot d\Omega\hat{\theta}^a(p) + \int_{\Omega_s} \frac{1}{\kappa(\boldsymbol{x})}\overline{F}(\boldsymbol{x}, p)\tilde{\theta}^*(\boldsymbol{x}, \boldsymbol{y}^b)d\Omega, \\ &\quad \text{for } \boldsymbol{y}^b\in\Omega \end{aligned} \tag{18}$$

and

$$\begin{aligned}&\sum_{a=1}^{n} \{\phi^a(\zeta^b) + \lim_{y\to\zeta^b}\int_{\Gamma_s} \frac{\partial\tilde{\theta}^*}{\partial n}(\boldsymbol{x}, \boldsymbol{y})\phi^a(\boldsymbol{x})d\Gamma \\ &\quad + \int_{L_s} \frac{\partial\tilde{\theta}^*}{\partial n}(\boldsymbol{x}, \zeta^b)\phi^a(\boldsymbol{x})d\Gamma \\ &\quad - \int_{\Gamma_s} n_k\phi^a_{,k}(\boldsymbol{x})\tilde{\theta}^*(\boldsymbol{x}, \zeta^b)d\Gamma\}\hat{\theta}^a(p) \\ &= - \sum_{a=1}^{n} \int_{\Omega_s} \tilde{\theta}^*(\boldsymbol{x}, \zeta^b)[\frac{p}{\kappa(\boldsymbol{x})}\phi^a(\boldsymbol{x}) - \frac{k_{,i}}{k}(\boldsymbol{x})\phi^a_{,i}(\boldsymbol{x})] \\ &\quad \cdot d\Omega\hat{\theta}^a(p) + \int_{\Omega_s} \frac{1}{\kappa(\boldsymbol{x})}\overline{F}(\boldsymbol{x}, p)\,\tilde{\theta}^*(\boldsymbol{x}, \zeta^b)d\Omega, \\ &\quad \text{for } \zeta^b\in\Gamma_q \end{aligned} \tag{19}$$

where Γ_q is a finite part of the global boundary Γ, over which the heat flux is prescribed. If the temperature is prescribed on a finite part, Γ_θ, the system of Eqs. (18) and (19) is supplemented by the approximation formula

$$\sum_{a=1}^{n} \phi^a(\boldsymbol{x})\hat{\theta}^a(p) = \bar{\tilde{\theta}}(\zeta^b, p), \text{ for } \zeta^b \in \Gamma_\theta$$

where $\bar{\tilde{\theta}}(\zeta^b, p)$ is the prescribed Laplace transform of the temperature.

It should be noted here that smaller size subdomains may induce larger oscillations or indentations in the shape functions derived from the meshless interpolations (Atluri and Shen, 2002). These characteristics of the interpolations are directly related to the difficulties in the numerical integration in Eqs. (18) and (19). To overcome these difficulties the integration domain is divided into smaller partitions. On each partition the standard Gaussian quadrature is applied. The sensitivity of the "final" solution with respect to the number of integration cells and the convergence properties in potential and elasticity theory in the so-called boundary node method have been discussed by Chati *et al*. (2001).

The time dependent values of the Laplace transformed variables can be obtained by an inverse Laplace transform. There are many inversion methods available for Laplace transform. As the inversion of the Laplace transform is an ill-posed problem, small truncation errors can be greatly magnified in the inversion process and lead to poor numerical results. Hence, special attention has to be paid in performing the inverse Laplace transform numerically. In the present analysis, Stehfest's inversion algorithm (Stehfest, 1970) is used. For certain types of problems like all those studied in this paper it is a stable and accurate method. However, it may fail badly for problems when their solution exhibits highly oscillatory behaviour.

2. Time Difference Formulation

In this approach, we use the linear interpolation for the time variation of the temperature field and the partial differential Eq. (1) is then reduced to the following system of equations:

$$\theta^{(n)}_{,ii}(\boldsymbol{x}) - \frac{1}{\kappa(\boldsymbol{x})\Delta t}\theta^{(n)}(\boldsymbol{x}) + \frac{1}{\kappa(\boldsymbol{x})\Delta t}\theta^{(n-1)}(\boldsymbol{x}) + \frac{k_{,i}}{k}(\boldsymbol{x})\theta^{(n)}_{,i}(\boldsymbol{x}) = -\frac{Q}{\kappa}(\boldsymbol{x}, t), \ (n=1, 2, \cdots, N) \quad (20)$$

where the backward difference scheme for the time derivative of the temperature is applied, and $\theta^{(n)}(\boldsymbol{x})$ denotes the value of the temperature at a point $\boldsymbol{x}$ and the time instant $t_n=n\Delta t$. For uniform time steps we have $\theta^{(n)}(\boldsymbol{x})=\theta(\boldsymbol{x}, n\Delta t)$. The solution of Eq. (20) can be expressed in an integral form. Following the procedure used in the previous section one can derive an integral representation for the temperature field at the n-th time step as

$$\begin{aligned}\theta^{(n)}(\boldsymbol{y}) = &\int_\Gamma \frac{\partial\theta^{(n)}}{\partial n}(\boldsymbol{x})\theta^*(\boldsymbol{x}, \boldsymbol{y})d\Gamma \\ &- \int_\Gamma \theta^{(n)}(\boldsymbol{x})\frac{\partial\theta^*}{\partial n}(\boldsymbol{x}, \boldsymbol{y})d\Gamma \\ &- \frac{1}{\Delta t}\int_\Omega \frac{1}{\kappa(\boldsymbol{x})}\theta^{(n)}(\boldsymbol{x})\theta^*(\boldsymbol{x}, \boldsymbol{y})d\Omega \\ &+ \frac{1}{\Delta t}\int_\Omega \frac{1}{\kappa(\boldsymbol{x})}\theta^{(n-1)}(\boldsymbol{x})\theta^*(\boldsymbol{x}, \boldsymbol{y})d\Omega \\ &+ \int_\Omega \frac{k_{,i}}{k}(\boldsymbol{x})\theta^{(n)}_{,i}(\boldsymbol{x})\theta^*(\boldsymbol{x}, \boldsymbol{y})d\Omega \end{aligned} \quad (21)$$

where the fundamental solution satisfies the Poisson's Eq. (4), and the body heat source is assumed to be absent.

If $\kappa=const$, the third and the fourth integral in Eq. (21) could be eliminated by using the fundamental solution

$$\theta^*(\boldsymbol{x}, \boldsymbol{y}) = \frac{1}{2\sqrt{\kappa\Delta t}}K_0(\sqrt{\kappa\Delta t}\,|\boldsymbol{x}-\boldsymbol{y}|) \quad (22)$$

where $K_0(z)$ is the modified Bessel function of the second kind and zeroth order. The fundamental solution (22) corresponds to the governing equation .

$$\theta^*_{,ii}(\boldsymbol{x}, \boldsymbol{y}) - \frac{1}{\kappa\Delta t}\theta^*(\boldsymbol{x}, \boldsymbol{y}) = -\delta(\boldsymbol{x}, \boldsymbol{y})$$

The last domain integral in Eq. (21) cannot be eliminated in the case of a general nonhomogeneous solid. Therefore, we use the integral representation (21) and the modified fundamental solution (7) instead of (22), which simplifies the numerical implementation. Similarly to the Laplace transform formulation it is convenient to introduce the LBIEs corresponding to the boundary-domain integral representation (21). Using the modified fundamental solution $\tilde{\theta}^*(r)$ given in Eq. (7) for a circular subdomain, we obtain a system of LBIEs for computing the discrete temperature values $\theta^{(n)}(\boldsymbol{y})$, $(n=1, 2, \cdots, N)$

$$\begin{aligned}\theta^{(n)}(\boldsymbol{y}) = &-\int_{\partial\Omega_s} \theta^{(n)}(\boldsymbol{x})\frac{\partial\tilde{\theta}^*}{\partial n}(\boldsymbol{x}, \boldsymbol{y})d\Gamma \\ &- \frac{1}{\Delta t}\int_{\Omega_s} \frac{1}{\kappa(\boldsymbol{x})}\theta^{(n)}(\boldsymbol{x})\tilde{\theta}^*(\boldsymbol{x}, \boldsymbol{y})d\Omega \\ &+ \frac{1}{\Delta t}\int_{\Omega_s} \frac{1}{\kappa(\boldsymbol{x})}\theta^{(n-1)}(\boldsymbol{x})\tilde{\theta}^*(\boldsymbol{x}, \boldsymbol{y})d\Omega \\ &+ \int_{\Omega_s} \frac{k_{,i}}{k}(\boldsymbol{x})\theta^{(n)}_{,i}(\boldsymbol{x})\tilde{\theta}^*(\boldsymbol{x}, \boldsymbol{y})d\Omega \end{aligned} \quad (23)$$

at $\boldsymbol{y}\in\Omega$. For $\boldsymbol{y}=\zeta\in\Gamma$ the LBIE takes the following form

$$\theta^{(n)}(\boldsymbol{y}) = -\int_{L_s}\theta^{(n)}(\boldsymbol{x})\frac{\partial\tilde{\theta}^*}{\partial n}(\boldsymbol{x},\zeta)d\Gamma - \lim_{y\to\zeta}\int_{\Gamma_s}\theta^{(n)}(\boldsymbol{x})\frac{\partial\tilde{\theta}^*}{\partial n}(\boldsymbol{x},\boldsymbol{y})d\Gamma + \int_{\Gamma_s}\frac{\partial\theta^{(n)}}{\partial n}(\boldsymbol{x})\tilde{\theta}^*(\boldsymbol{x},\zeta)d\Gamma - \frac{1}{\Delta t}\int_{\Omega_s}\frac{1}{\kappa(\boldsymbol{x})}\theta^{(n)}(\boldsymbol{x})\tilde{\theta}^*(\boldsymbol{x},\zeta)d\Omega + \frac{1}{\Delta t}\int_{\Omega_s}\frac{1}{\kappa(\boldsymbol{x})}\theta^{(n-1)}(\boldsymbol{x})\tilde{\theta}^*(\boldsymbol{x},\zeta)d\Omega + \int_{\Omega_s}\frac{k_{,i}}{k}(\boldsymbol{x})\theta^{(n)}_{,i}(\boldsymbol{x})\tilde{\theta}^*(\boldsymbol{x},\zeta)d\Omega \qquad (24)$$

For the first time step, i.e., n=1, the value $\theta^{(0)}(\boldsymbol{x})$ is given by the initial condition for the temperature distribution. Substituting the approximation formula (16) for the temperature field into Eqs. (23) and (24) one obtains a system of algebraic equations for the fictitious nodal unknowns $\hat{\theta}^{a(n)}$ at the discrete time instants

$$\sum_{a=1}^{n}\{\phi^a(\boldsymbol{y}^b) + \int_{\partial\Omega_s}\frac{\partial\tilde{\theta}^*}{\partial n}(\boldsymbol{x},\boldsymbol{y}^b)\phi^a(\boldsymbol{x})d\Gamma\}\hat{\theta}^{a(n)} = -\frac{1}{\Delta t}\sum_{a=1}^{n}\int_{\Omega_s}\frac{1}{\kappa(\boldsymbol{x})}\tilde{\theta}^*(\boldsymbol{x},\boldsymbol{y}^b)\phi^a(\boldsymbol{x})d\Omega[\hat{\theta}^{a(n)} - \hat{\theta}^{a(n-1)}] + \sum_{a=1}^{n}\int_{\Omega_s}\frac{k_{,i}}{k}(x)\tilde{\theta}^*(\boldsymbol{x},\boldsymbol{y}^b)\phi^a_{,i}(\boldsymbol{x})d\Omega\hat{\theta}^{a(n)} \quad \text{for } \boldsymbol{y}^b\in\Omega \qquad (25)$$

and

$$\sum_{a=1}^{n}\{\phi^a(\zeta^b) + \lim_{\boldsymbol{y}\to\zeta^b}\int_{\Gamma_s}\frac{\partial\tilde{\theta}^*}{\partial n}(\boldsymbol{x},\boldsymbol{y}^b)\phi^a(\boldsymbol{x})d\Gamma + \int_{L_s}\frac{\partial\tilde{\theta}^*}{\partial n}(\boldsymbol{x},\zeta^b)\phi^a(\boldsymbol{x})d\Gamma - \int_{\Gamma_s}n_k\phi^a_{,k}(\boldsymbol{x})\tilde{\theta}^*(\boldsymbol{x},\zeta^b)d\Gamma\}\hat{\theta}^{a(n)} = -\frac{1}{\Delta t}\sum_{a=1}^{n}\int_{\Omega_s}\frac{1}{\kappa(\boldsymbol{x})}\tilde{\theta}^*(\boldsymbol{x},\zeta^b)\phi^a(\boldsymbol{x})d\Omega[\hat{\theta}^{a(n)} - \hat{\theta}^{a(n-1)}] + \sum_{a=1}^{n}\int_{\Omega_s}\frac{k_{,i}}{k}(\boldsymbol{x})\tilde{\theta}^*(\boldsymbol{x},\zeta^b)\phi^a_{,i}(\boldsymbol{x})d\Omega\hat{\theta}^{a(n)} \quad \text{for } \xi^b\in\Gamma_q \qquad (26)$$

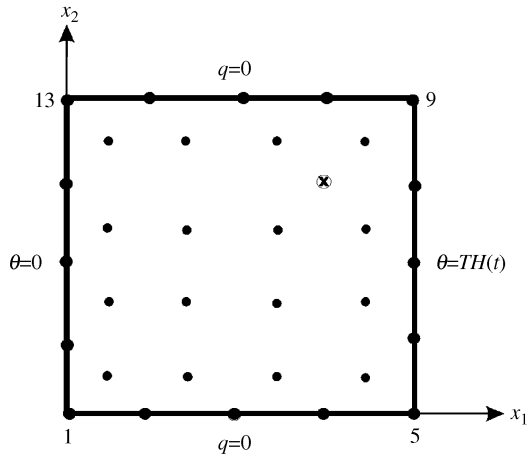

Fig. 1 Boundary conditions and node distribution for a square plate

For the prescribed temperature on a finite part Γ_θ, the system of Eqs. (25) and (26) is supplemented by the approximation formula

$$\sum_{a=1}^{n}\phi^a(\boldsymbol{x})\hat{\theta}^{a(n)} = \tilde{\theta}(\zeta^b, n\Delta t)\,, \text{ for } \zeta^b\in\Gamma_\theta \qquad (27)$$

Resolving the system of algebraic Eqs. (25)-(27) for the unknown fictitious nodal values $\hat{\theta}^{a(n)}$ time-step by time-step, the final physical temperature field at the discrete time instants can be obtained by Eq. (16).

3. Numerical Examples

In the LBIEM presented in this section, the spatial variation of the material properties of FGMs is allowed to be arbitrary. For illustration, we assume an exponential dependence of the material parameters on the Cartesian coordinates, which is frequently utilized for modelling FGMs (Noda and Jin, 1993; Jin and Batra, 1996). In this special case the governing equations for heat conduction problems are substantially simplified in comparison to a general nonhomogeneous case. In particular, we use a unidirectional variation for the thermal conductivity and diffusivity coefficients

$$k(\boldsymbol{x})=k_0e^{\gamma x_1};\ \kappa(\boldsymbol{x})=\kappa_0e^{\gamma x_1}$$

(i) A Homogeneous Square Plate

As our first example, a square plate with homogeneous material properties is analyzed (see Fig. 1). On the opposite sides parallel to the x_2-axis, different temperatures are prescribed. One side is kept to zero temperature while the other side is subjected to a Heaviside-type thermal loading $\theta(x_2, t)=T\,H(t)$ with T=1 deg. On the other side of the plate, the heat flux

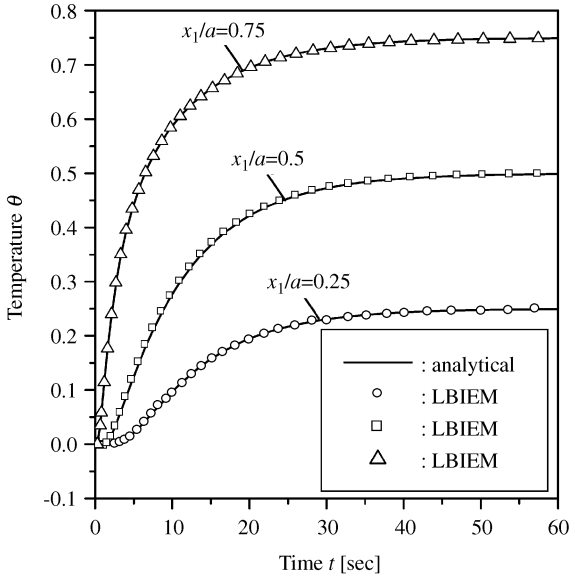

Fig. 2 Time variation of the temperature computed at three points by the Laplace transform LBIEM

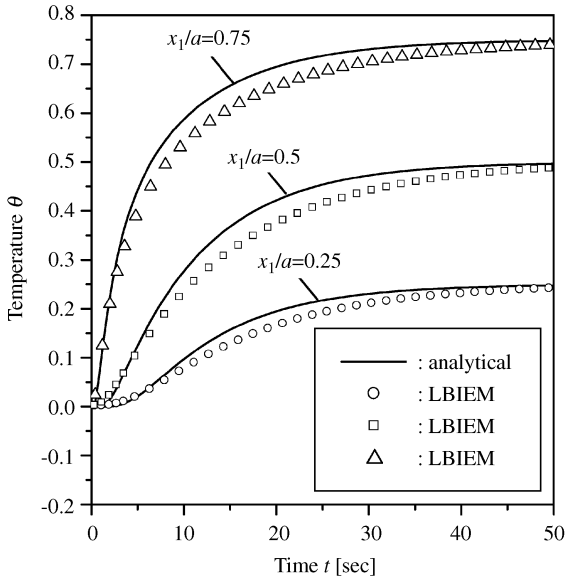

Fig. 3 Time variation of the temperature in a square plate obtained by the time difference LBIEM

is vanishing. The initial temperature is assumed to be zero throughout the whole body. In our numerical calculations we have considered a side length a= 0.04m and a thermal diffusivity parameter $\kappa=\kappa_0=0.17\times10^{-4}$ m^{2}s^{-1}. In the meshless LBIEM, 16 nodes on the boundary and 16 nodes inside the investigated domain have been used. A regular node distribution is first applied (see Fig. 1). The radius of a circular subdomain is selected as $r_{loc}=0.39\times10^{-2}$ m. Numerical results are compared with the analytical solution given by (Carslaw and Jaeger, 1959)

$$\theta(x_1, t) = T\frac{x_1}{a} + \frac{2}{\pi}\sum_{n}^{\infty}\frac{T\cos n\pi}{n}\sin\frac{n\pi x_1}{a}\exp(-\frac{\kappa n^2\pi^2 t}{a^2}) \tag{28}$$

The comparison of analytical and numerical results is made at three locations lying on the x_1-axis with x_1/a=0.25, 0.5 and 0.75. Numerical results provided by Laplace transform LBIEM are presented in Fig. 2. For numerical inversion of Laplace transform we have used 15 different Laplace transform parameters. Fig. 2 shows an excellent agreement between numerical and analytical results. A little worse agreement is noted for the numerical results obtained by the time difference LBIEM. The time step was selected, for the whole time interval, as Δt=0.4 sec. The corresponding numerical results obtained by in the time difference LBIEM are presented in Fig. 3. One way to increase the accuracy of the numerical scheme is the use of the following second order backward difference scheme for the time derivative of the temperature in the governing Eq. (1) (Curran *et al.*, 1980)

$$\frac{\partial\theta^{(n+1)}}{\partial t} \cong \frac{3\theta^{(n+1)} - 4\theta^{(n)} + \theta^{(n-1)}}{\Delta t}.$$

For the purpose of error estimation and convergence studies, the Sobolev norm is calculated. Accordingly, the relative error for the temperature is defined as

$$r_t = \frac{\left\| \theta^{num} - \theta^{exact} \right\|}{\left\| \theta^{exact} \right\|} \tag{29}$$

where

$$\left\| \theta \right\| = (\int_{\Omega} \theta^2 d\Omega)^{1/2}$$

The relative error can be computed at various time instants. To study the convergence of the proposed method we have used three regular node distributions in the MSL approximation (see Fig. 1) with 21 (12 boundary + 9 interior), 32 (16 boundary + 16 interior) and 45 (20 boundary + 25 interior) nodes, respectively. For a regular node distribution, the density of nodes can be characterized by the distance of two neighbouring nodes s. The relative errors of the numerically computed temperature at two different time instants t=10 and 30 sec, with respect to the exact values of the temperature, are shown in Fig. 4. It can be seen that the present meshless LBIEM has a high convergence rate at both time instants considered. The results are sufficiently accurate, with a relative error of about 0.1% for the finest node distribution.

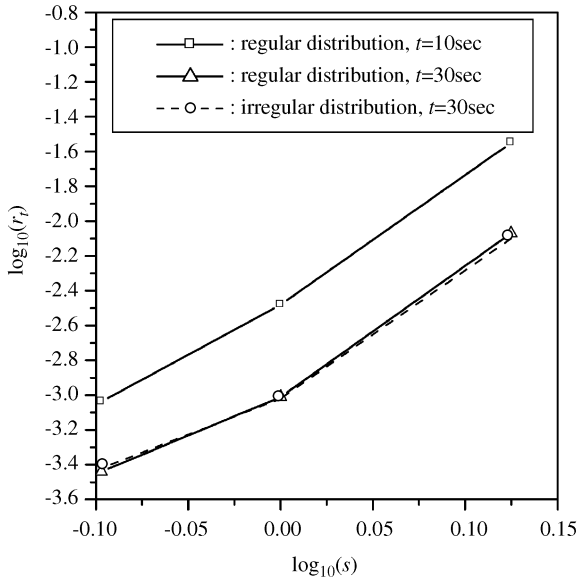

Fig. 4 Relative errors and convergence rates of the temperature at two different time instants for regular and irregular node distributions

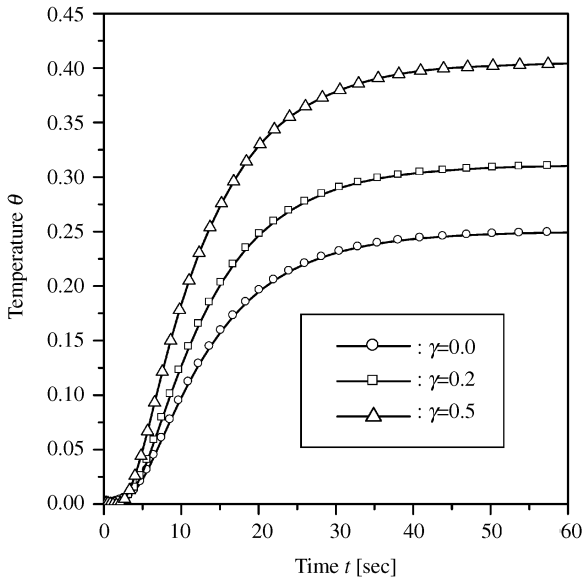

Fig. 5 Time variation of the temperature at the point of x_1/a= 0.25 of an FGM square plate

The influence of the irregular node distribution on the accuracy is analysed too. In the vicinity of the corner node 9 in Fig. 1, an additional node, indicated by the cross sign, is added into the previous regular node distribution. For simplicity, only one node is used to destroy the regularity of the node distribution. The coordinates of the additional node for the coarse, middle and finest node distributions are (0.0267, 0.0267) , (0.03, 0.03) and (0.032, 0.032), respectively. Fig. 4 shows very similar relative errors and convergence rates for both regular and irregular node distributions. Since the size of the subdomains is considered to be the same in both cases, the number of integration partitions for the integration domain is the same too. It means that the CPU is the same in both considered regular and irregular node distributions. However, for a finer node distribution the size of the subdomains is smaller than that for the coarser one. Thus, the number of integration partitions is generally higher and the required CPU is increased.

(ii) An FGM Square Plate

To illustrate the applicability of the proposed LBIEM to nonhomogeneous solids, an FGM square plate with an exponential variation of the thermal conductivity and diffusivity is analyzed numerically. Numerical calculations have been carried out for the following material constants $\kappa_0=0.17\times10^{-4}$ m^2s^{-1}, $k_0=17$ $Wm^{-1}deg^{-1}$, and two different exponential parameters $\gamma=0.2$ and 0.5 cm^{-1}. The problem was analysed by the Laplace transform LBIEM. The geometry and the used node distribution are the same as in the previously investigated homogeneous case. The time variation of the temperature at the point $x_1/a=0.25$ for three γ-values is presented in Fig. 5. Here, $\gamma=0$ corresponds to the homogeneous case. With increasing γ-value the thermal conductivity is increasing too, and a higher level of temperature at the considered point is obtained in the stationary state, i.e., $t=\infty$. For stationary state one can derive an analytical solution as

$$\theta(x_1) = T\frac{e^{-\gamma x_1}-1}{e^{-\gamma a}-1}$$

Numerical results given in Fig. 5 approach the analytical ones at a sufficiently large time value, e.g., $t>$ 60 sec.

III. 3-D AXISYMMETRIC HEAT CONDUCTION PROBLEMS

For a 3-d axisymmetric problem it is convenient to use cylindrical coordinates (r, φ, z). In such a case the governing Eq. (1) can be rewritten into the form

$$\frac{\partial^2\theta}{\partial r^2}(r,z,t)+\frac{\partial^2\theta}{\partial z^2}(r,z,t)+\frac{1}{r}\frac{\partial\theta}{\partial r}(r,z,t)$$

$$-\frac{1}{\kappa(r,z)}\frac{\partial\theta}{\partial t}(r,z,t)+\frac{k_{,\alpha}}{k}(r,z)\theta_{,\alpha}(r,z,t)$$

$$=-\frac{1}{\kappa(r,z)}Q(r,z,t) \qquad (30)$$

where the summation convention for repeated

indices α, representing the coordinates r and z, is used.

Applying the Laplace transform to Eq. (30) we get

$$\frac{\partial^2 \overline{\theta}}{\partial r^2}(r, z, p) + \frac{\partial^2 \overline{\theta}}{\partial z^2}(r, z, p) + \frac{1}{r}\frac{\partial \overline{\theta}}{\partial r}(r, z, p) - \frac{p}{\kappa(r, z)}\overline{\theta}(r, z, p) + \frac{k_{,\alpha}}{k}(r, z)\overline{\theta}_{,\alpha}(r, z, p) = -\frac{1}{\kappa(r, z)}\overline{F}(r, z, p) \tag{31}$$

where

$$\overline{F}(r, z, p) = \overline{Q}(r, z, p) + \theta(r, z, 0)$$

is the redefined body heat source in the Laplace transformed domain with the initial boundary condition for the temperature field $\theta(r, z, 0)$.

The solution of the governing Eq. (31) can be found in a weak form with a fundamental solution

$$\theta^*(\boldsymbol{s}, \boldsymbol{q}) = \frac{1}{2\pi}\ln\frac{1}{\rho} \tag{32}$$

corresponding to the Poisson's equation

$$\frac{\partial^2 \theta^*}{\partial r^2} + \frac{\partial^2 \theta^*}{\partial z^2} = -\delta(\boldsymbol{s}, \boldsymbol{q})$$

where ρ is the distance of the field and the source points, i.e., $\rho=|\boldsymbol{s}-\boldsymbol{q}|$.

By the application of the Gauss divergence theorem to the weak form of Eq. (31) we obtain an integral representation for the temperature field in the Laplace transform domain

$$\begin{aligned}\overline{\theta}(\boldsymbol{q}, p) = &\int_{\Gamma} \frac{\partial \overline{\theta}}{\partial n}(\boldsymbol{s}, p)\theta^*(\boldsymbol{s}, \boldsymbol{q})d\Gamma \\ &- \int_{\Gamma} \overline{\theta}(\boldsymbol{s}, p)\frac{\partial \theta^*}{\partial n}(\boldsymbol{s}, \boldsymbol{q})d\Gamma \\ &+ \int_{\Omega} \frac{1}{r}\frac{\partial \overline{\theta}}{\partial r}(\boldsymbol{s}, p)\theta^*(\boldsymbol{s}, \boldsymbol{q})d\Omega \\ &- \int_{\Omega} \frac{p}{\kappa(\boldsymbol{s})}\overline{\theta}(\boldsymbol{s}, p)\theta^*(\boldsymbol{s}, \boldsymbol{q})d\Omega \\ &+ \int_{\Omega} \frac{k_{,\alpha}}{k}(\boldsymbol{s})\overline{\theta}_{,\alpha}(\boldsymbol{s}, p)\theta^*(\boldsymbol{s}, \boldsymbol{q})d\Omega \\ &+ \int_{\Omega} \frac{1}{\kappa(\boldsymbol{s})}\overline{F}(\boldsymbol{s}, p)\theta^*(\boldsymbol{s}, \boldsymbol{q})d\Omega \end{aligned} \tag{33}$$

where Γ is the boundary of the analysed domain Ω and r denotes the radial coordinate of the field point, i.e., $\boldsymbol{s}\equiv(r, z)$.

Since the boundary-domain integral representation (33) for the Laplace transform of the temperature contains the temperature gradients, the integral representation for the temperature gradients at interior points has to be added to obtain a unique integral formulation.

Like in the previous 2-d problems it is more convenient to use the LBIE

$$\begin{aligned}\overline{\theta}(\boldsymbol{q}, p) = &\int_{\partial\Omega_s} \frac{\partial \overline{\theta}}{\partial n}(\boldsymbol{s}, p)\theta^*(\boldsymbol{s}, \boldsymbol{q})d\Gamma \\ &- \int_{\partial\Omega_s} \overline{\theta}(\boldsymbol{s}, p)\frac{\partial \theta^*}{\partial n}(\boldsymbol{s}, \boldsymbol{q})d\Gamma \\ &+ \int_{\Omega_s} \frac{1}{r}\frac{\partial \overline{\theta}}{\partial r}(\boldsymbol{s}, p)\theta^*(\boldsymbol{s}, \boldsymbol{q})d\Omega \\ &- \int_{\Omega_s} \frac{p}{\kappa(\boldsymbol{s})}\overline{\theta}(\boldsymbol{s}, p)\theta^*(\boldsymbol{s}, \boldsymbol{q})d\Omega \\ &+ \int_{\Omega_s} \frac{k_{,\alpha}}{k}(\boldsymbol{s})\overline{\theta}_{,\alpha}(\boldsymbol{s}, p)\theta^*(\boldsymbol{s}, \boldsymbol{q})d\Omega \\ &+ \int_{\Omega_s} \frac{1}{\kappa(\boldsymbol{s})}\overline{F}(\boldsymbol{s}, p)\theta^*(\boldsymbol{s}, \boldsymbol{q})d\Omega \end{aligned} \tag{34}$$

The integral Eq. (34) is considered for small subdomains $\Omega_s\subset\Omega$. Hence, none of the boundary densities in the Laplace transformed domain are prescribed on the local boundary $\partial\Omega_s$ as long as they lie entirely inside Ω. To reduce the number of the unknowns on $\partial\Omega_s$ the concept of a companion solution is utilized (Zhu *et al.*, 1998). The modified test function

$$\tilde{\theta}^*(\boldsymbol{x}, \boldsymbol{y}) = \frac{1}{2\pi}\ln\frac{\rho_0}{\rho} \tag{35}$$

is the Green's function vanishing on the boundary of the circular subdomain of radius ρ_0. Since the integral Eq. (34) is also valid for the modified fundamental solution $\tilde{\theta}^*(\boldsymbol{s}, \boldsymbol{q})$, we obtain

$$\begin{aligned}\overline{\theta}(\boldsymbol{q}, p) = &-\int_{\partial\Omega_s} \overline{\theta}(\boldsymbol{s}, p)\frac{\partial \tilde{\theta}^*}{\partial n}(\boldsymbol{s}, \boldsymbol{q})d\Gamma \\ &+ \int_{\Omega_s} \frac{1}{r}\frac{\partial \overline{\theta}}{\partial r}(\boldsymbol{s}, p)\tilde{\theta}^*(\boldsymbol{s}, \boldsymbol{q})d\Omega \\ &- \int_{\Omega_s} \frac{p}{\kappa(\boldsymbol{s})}\overline{\theta}(\boldsymbol{s}, p)\tilde{\theta}^*(\boldsymbol{s}, \boldsymbol{q})d\Omega \\ &+ \int_{\Omega_s} \frac{k_{,\alpha}}{k}(\boldsymbol{s})\overline{\theta}_{,\alpha}(\boldsymbol{s}, p)\tilde{\theta}^*(\boldsymbol{s}, \boldsymbol{q})d\Omega \\ &+ \int_{\Omega_s} \frac{1}{\kappa(\boldsymbol{s})}\overline{F}(\boldsymbol{s}, p)\tilde{\theta}^*(\boldsymbol{s}, \boldsymbol{q})d\Omega \end{aligned} \tag{36}$$

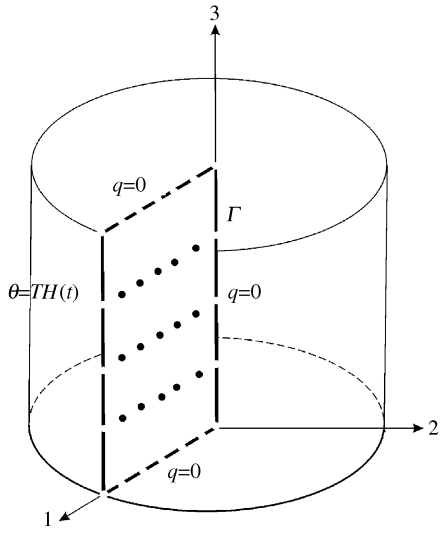

Fig. 6 Boundary conditions and node distribution in the analyzed domain for a finite cylinder

for the interior source point $\boldsymbol{q}\in\Omega$, and

$$\overline{\theta}(\zeta, p) = -\int_{L_s} \overline{\theta}(\boldsymbol{s}, p)\frac{\partial\tilde{\theta}^*}{\partial n}(\boldsymbol{s}, \zeta)d\Gamma - \lim_{\boldsymbol{q}\to\zeta}\int_{\Gamma_s} \overline{\theta}(\boldsymbol{s}, p)\frac{\partial\tilde{\theta}^*}{\partial n}(\boldsymbol{s}, \boldsymbol{q})d\Gamma + \int_{\Gamma_s}\frac{\partial\overline{\theta}}{\partial n}(\boldsymbol{s}, p)\tilde{\theta}^*(\boldsymbol{s}, \zeta)d\Gamma + \int_{\Omega_s}\frac{1}{r}\frac{\partial\overline{\theta}}{\partial r}(\boldsymbol{s}, p)\tilde{\theta}^*(\boldsymbol{s}, \zeta)d\Omega - \int_{\Omega_s}\frac{p}{\kappa}\overline{\theta}(\boldsymbol{s}, p)\tilde{\theta}^*(\boldsymbol{s}, \zeta)d\Omega + \int_{\Omega_s}\frac{k_{,\alpha}}{k}(s)\overline{\theta}_{,\alpha}(\boldsymbol{s}, p)\tilde{\theta}^*(\boldsymbol{s}, \zeta)d\Omega + \int_{\Omega_s}\frac{1}{\kappa}\overline{F}(\boldsymbol{s}, p)\tilde{\theta}^*(\boldsymbol{s}, \zeta)d\Omega \qquad (37)$$

for the source point located on the global boundary $\zeta\in\Gamma_s\subset\Gamma$. Note here that $\partial\Omega_s=L_s\cup\Gamma_s$, where L_s is the circular part of $\partial\Omega_s$ (Zhu *et al.*, 1998). The integral Eq. (37) is written in the limit form. Such an expression is appropriate (Sladek *et al.*, 2000) if the physical fields such as the temperature are given in a non-polynomial approximation form.

Again the MLS approximation is used for the numerical solution of the LBIEs. The approximation formulae for the Laplace transform of the temperature and its normal derivative are given by Eqs. (16) and (17). Substituting the approximation formulae (16) and (17) into the LBIEs (36) and (37) we obtain a set of linear algebraic equations

$$\sum_{i=1}^{n}\{\phi^i(\boldsymbol{q}^b) + \int_{\partial\Omega_s}\frac{\partial\tilde{\theta}^*}{\partial n}(\boldsymbol{s}, \boldsymbol{q}^b)\phi^i(\boldsymbol{s})d\Gamma + \int_{\Omega_s}\tilde{\theta}^*(\boldsymbol{x}, \boldsymbol{q}^b)\cdot[\frac{p}{\kappa}\phi^i(\boldsymbol{s}) - \frac{1}{r}\phi^i_{,r}(\boldsymbol{s}) - \frac{k_{,\alpha}}{k}(\boldsymbol{s})\phi^i_{,\alpha}(\boldsymbol{s})]d\Omega\}\cdot\hat{\theta}^i(p) = \int_{\Omega_s}\frac{1}{\kappa}\overline{F}(\boldsymbol{s}, p)\tilde{\theta}^*(\boldsymbol{s}, \boldsymbol{q}^b)d\Omega, \text{ for } \boldsymbol{q}^b\in\Omega \qquad (38)$$

and

$$\sum_{i=1}^{n}\{\phi^i(\zeta^b) + \lim_{\boldsymbol{q}\to\zeta^b}\int_{\Gamma_s}\frac{\partial\tilde{\theta}^*}{\partial n}(\boldsymbol{s}, \boldsymbol{q})\phi^i(\boldsymbol{s})d\Gamma + \int_{L_s}\frac{\partial\tilde{\theta}^*}{\partial n}(s, \zeta^b)\phi^i(\boldsymbol{s})d\Gamma + \int_{\Omega_s}\tilde{\theta}^*(\boldsymbol{s}, \zeta^b)[\frac{p}{\kappa}\phi^i(\boldsymbol{s}) - \frac{1}{r}\phi^i_{,r}(\boldsymbol{s}) - \frac{k_{,\alpha}}{k}(\boldsymbol{s})\phi^i_{,\alpha}(\boldsymbol{s})]d\Omega\}\cdot\hat{\theta}^i(p) = \int_{\Gamma_s}\frac{\partial\overline{\theta}}{\partial n}(\boldsymbol{s}, p)\tilde{\theta}^*(\boldsymbol{s}, \zeta^b)d\Gamma + \int_{\Omega_s}\frac{1}{\kappa}\overline{F}(\boldsymbol{s}, p)\tilde{\theta}^*(\boldsymbol{s}, \zeta^b)d\Omega, \text{ for } \zeta^b\in\Gamma_s\cap\Gamma_q \qquad (39)$$

where Γ_q is a part of the global boundary Γ, over which the heat flux is prescribed. If the temperature is prescribed on a part Γ_θ we propose to collocate the approximation formula (16) by using

$$\sum_{i=1}^{n}\phi^i(\zeta^b)\hat{\theta}^i(p) = \overline{\theta}(\zeta^b, p), \text{ for } \zeta^b\in\Gamma_\theta \qquad (40)$$

where $\overline{\theta}(\zeta^b, p)$ is the Laplace transform of the prescribed temperature.

The time-dependent values of the transformed quantities in the previous consideration can be obtained by an inverse Laplace transform. As in the 2-d analysis, the sophisticated Stehfest's algorithm (Stehfest, 1970) for the numerical inversion is used.

1. Numerical Examples

(i) Full Cylinder

An infinitely long full cylinder with a radius a=1 m loaded by a thermal shock $\theta(a, t)=TH(t-0)$ with T=100 deg as shown in Fig. 6 is first considered. In the first example, homogeneous material properties

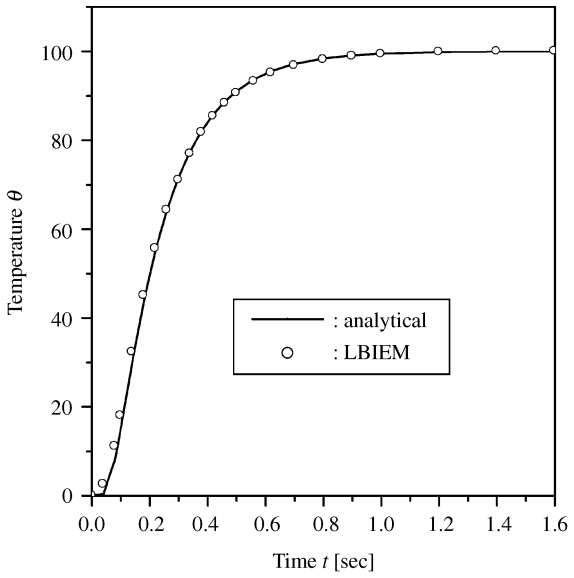

Fig. 7 Time variation of the temperature on the axis of a homogeneous cylinder

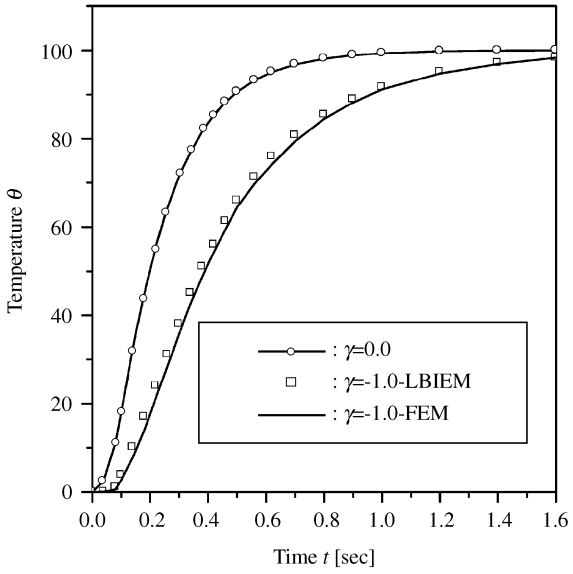

Fig. 8 Comparison of the time variations of the temperature in an infinite homogeneous (γ=0) and an FGM cylinder

are assumed in the numerical analysis to check the accuracy of the LBIEM. The diffusivity coefficient is chosen as κ=1 m^{2}s^{-1}. Since the boundary conditions along the cylinder are uniform we can consider a finite part of the cylinder in the numerical analysis with prescribed vanishing heat fluxes on both artificial cross sections of the cylinder (Fig.6). The cylindrical surface can be created by the rotation of a rectangular plate of the size ($a\times L$), where a is the radius and 2L is the length of the cylinder. Here, L=1m is chosen. The temperature field on the finite square region is modelled by 20 boundary and 15 interior nodes (see Fig. 6). Numerical results are compared with the following analytical solution (Carslaw and Jaeger, 1959)

$$\theta(r,t) = T - \frac{2T}{a}\sum_{n=1}^{\infty} T\frac{J_0(r\alpha_n)}{\alpha_n J_1(a\alpha_n)}\exp(-\kappa\alpha_n^2 t) \quad (41)$$

where $J_0(a\alpha_n)$ is the Bessel function of the first kind and zeroth order, and α_n are the roots of the following transcendental equation

$$J_0(a\alpha_n)=0$$

The time variation of the temperature on the axis of the cylinder is presented in Fig. 7, where an excellent agreement between numerical and analytical results is obtained.

Next we proceed to consider a functionally graded full cylinder. To protect the cylinder against a drastic thermal shock the thermal conductivity and diffusivity should be decreasing in the radial direction. In our numerical calculations, an exponential spatial variation for both parameters

$$k(\boldsymbol{x})=k_0 e^{\gamma r}$$

$$\kappa(\boldsymbol{x})=\kappa_0 e^{\gamma r} \quad (42)$$

has been assumed with $\kappa_0=0.17\times10^{-4}$ m^{2}s^{-1}, k_0=17 Wm^{-1} deg^{-1} and γ=-1 m^{-1}.

Numerical results provided by the LBIEM are compared with those obtained by the FEM-code MSC/NASTRAN. A very fine mesh discretization with 16 linear solid elements in the radial direction was used in the FEM. The total number of elements for a quarter of the cylinder is 320. The time variation of the temperature at the center of the cylinder is presented in Fig. 8 for both methods. One can see a good agreement of both numerical results. Fig. 8 shows that the temperature evolution for a homogeneous cylinder with γ=0 is steeper than that for the functionally graded cylinder with decreasing thermal parameters in the radial direction.

(ii) Hollow Cylinder

In the next example, an infinitely long functionally graded thick-walled hollow cylinder with the radii $R_1=8\times10^{-2}$ m and $R_2=10\times10^{-2}$ m as depicted in Fig. 9 is investigated. As boundary condition on the external surface of the hollow cylinder the Heaviside time variation for the time-dependent thermal loading is assumed as a thermal shock. The inner surface is kept at zero temperature. The corresponding

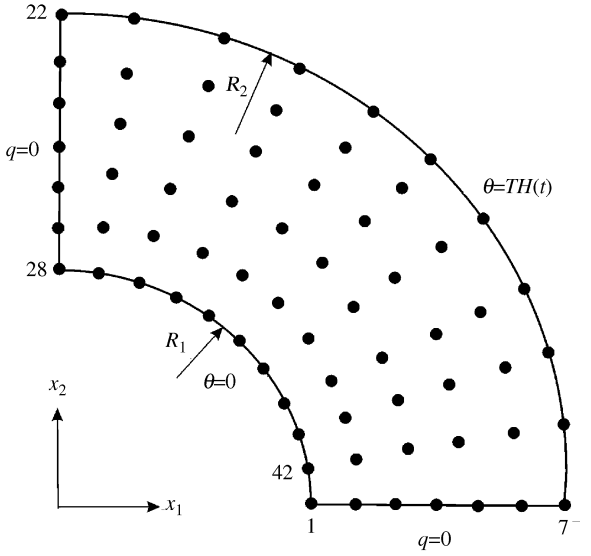

Fig. 9 Boundary conditions and node distribution for an infinite hollow cylinder

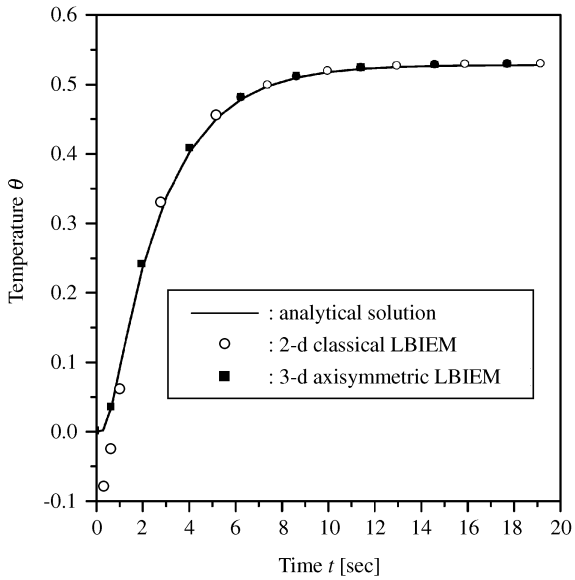

Fig.10 Time variations of the temperature at r=9.0 cm in a homogeneous hollow cylinder

boundary value problem can be analysed as a 2-d problem for a cross-section of the cylinder, which is referred to as the classical 2-d LBIEM in the following. Due to the symmetry in geometry and boundary conditions it is sufficient to analyze only a quarter of the cross-section of the hollow cylinder as shown in Fig. 9. The total number of nodes used for the MLS approximation is 84 with 42 nodes lying on the global boundary as depicted in Fig. 9. For comparison purpose, a homogeneous hollow cylinder is first considered. The values of the thermal diffusivity κ_0=0.17×10^{-4} m^{2}s^{-1} and conductivity k_0=17 Wm^{-1}deg^{-1} are used in the numerical analysis. Alternatively, the considered boundary value problem can be analysed as a 3-d axisymmetric problem too. A finite part of the hollow cylinder can be obtained by the rotation of the rectangular region around the z-axis. In the LBIEM the rectangular region with the coordinates (r, z) is modelled by 40 nodes. The time variation of the temperature at the radius r= 9 cm is presented in Fig. 10. Numerical results are compared with the analytical solution (Carslaw and Jaeger, 1959)

$$\theta(r,t) = T\frac{\ln(r/R_1)}{\ln(R_2/R_1)} - \pi\sum_{n=1}^{\infty} T\frac{J_0^2(R_1\alpha_n)U_0(r\alpha_n)}{J_0^2(R_1\alpha_n) - J_0^2(R_2\alpha_n)} \cdot \exp(-\kappa\alpha_n^2 t) \quad (43)$$

where

$$U_0(r\alpha_n)=J_0(r\alpha_n)Y_0(\alpha_n R_2)-J_0(\alpha_n R_2)Y_0(r\alpha_n)$$

and α_n are the roots of the following transcendental equation

$$J_0(r)Y_0(rR_2/R_1)-J_0(rR_2/R_1)Y_0(r)=0$$

with $Y_0(x)$ being the Bessel function of second kind and zeroth order. Fig. 10 implies that a better accuracy is obtained by the 3-d axisymmetric LBIEM. The discrepancies between the numerical results obtained by the classical 2-d LBIEM and the 3-d axisymmetric LBIEM are observed at small time instants. The number of nodes in our numerical calculations in the 3-d axisymmetric LBIEM is approximately one half of that used in the classical 2-d LBIEM. This means that the 3-d axisymmetric LBIEM is computationally more efficient than the classical 2-d LBIEM.

Now, let us consider a functionally graded hollow cylinder with the thermal diffusivity and conductivity being graded in the radial direction r *as* described by Eq. (42). The applied parameters κ_0 and k_0 in Eq. (42) are the same as in the homogeneous case. For three values of the gradient parameter γ, numerical results for the time variation of the temperature at r=9 cm are shown in Fig. 11. The temperature level at interior points in the steady state (i.e., t=∞) increases with increasing γ-value. Compared to the temperature for a homogeneous hollow cylinder (i.e., γ=0), the temperature in a functionally graded hollow cylinder is higher.

IV. MICROWAVE HEATING ANALYSIS

Microwave heating of a continuously non-homogeneous body can be modelled by the non-stationary forced heat conduction equation, which is a

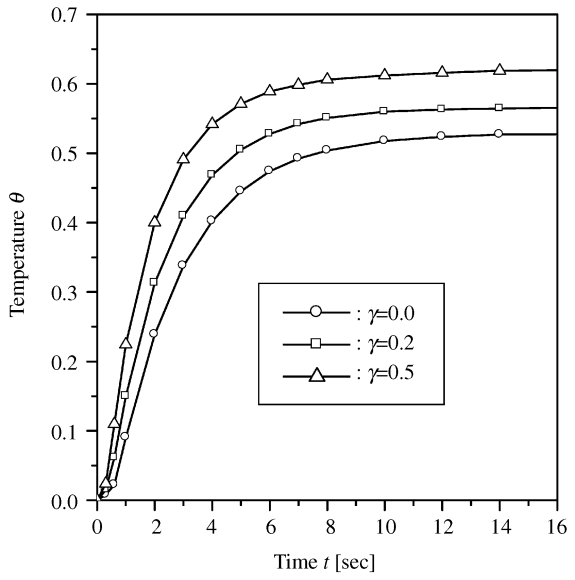

Fig.11 Time variations of the temperature at r=9.0 cm in an FGM hollow cylinder

generalized form of the homogeneous case (Zhu *et al*., 1995)

$$\theta_{,ii}(\boldsymbol{x}, t) - \frac{1}{\kappa(\boldsymbol{x})}\frac{\partial\theta}{\partial t}(\boldsymbol{x}, t) + \frac{k_{,i}}{k}(\boldsymbol{x})\theta_{,i}(\boldsymbol{x}, t)$$

$$= -\frac{1}{\kappa(\boldsymbol{x})}\beta(\theta)\left|E\right|^2 \tag{44}$$

where $\theta(\boldsymbol{x}, t)$ is the temperature field, k and κ represent the thermal conductivity and diffusivity coefficients, $\beta(\theta)$ is the thermal absorptivity coefficient and $|E|$ is the amplitude of the electric field, respectively. In the following analysis, the amplitude of the electric field is assumed to be exponentially dependent on the spatial variable z (Zhu *et al*., 1995), i.e.,

$$|E|=\exp(-\gamma z/2) \tag{45}$$

for decay from an incident boundary at z=0, where γ is a decay constant. The simplified model for microwave heating is then determined by

$$\theta_{,ii}(\boldsymbol{x}, t) - \frac{1}{\kappa(\boldsymbol{x})}\frac{\partial\theta}{\partial t}(\boldsymbol{x}, t) + \frac{k_{,i}}{k}(\boldsymbol{x})\theta_{,i}(\boldsymbol{x}, t)$$

$$= -\frac{1}{\kappa(\boldsymbol{x})}\beta(\theta)\exp(-\gamma z) \tag{46}$$

The microwave heating problem is described by a nonlinear parabolic partial differential Eq. (46). Analytical solutions exist only for simple geometrical and loading conditions, with uniform material properties and γ=0. For general cases, Eq. (46) has to be solved numerically. A dual reciprocity BEM (DRBEM) has been presented by Zhu *et al*. (1995), where numerical results are given for uniform material properties.

If the thermal absorptivity is a nonlinear function of temperature, a linearization scheme has to be applied to Eq. (46). This can be done by using the following first-order Taylor-series expansion (Ramachandran, 1990)

$$\beta(\theta) = \beta(\tilde{\theta}) + (\theta - \tilde{\theta})\left.\frac{\partial\beta}{\partial\theta}\right|_{\theta=\tilde{\theta}} \tag{47}$$

where $\tilde{\theta}$ is the previously iterated solution at a particular time.

To eliminate the time variable in the differential Eq. (46), the Laplace transform technique is used. Applying the Laplace transform to the linearized governing Eq. (46) we obtain

$$\overline{\theta}_{,ii}(\boldsymbol{x}, p) - \frac{p}{\kappa}\overline{\theta}(\boldsymbol{x}, p) + \frac{k_{,i}}{k}(\boldsymbol{x})\overline{\theta}_{,i}(\boldsymbol{x}, p)$$

$$+ f_1(\boldsymbol{x}, z, \tilde{\theta})\overline{\theta}(\boldsymbol{x}, p) = -\overline{F}(\boldsymbol{x}, p) \tag{48}$$

where

$$f_1(\boldsymbol{x}, z, \tilde{\theta}) = \frac{1}{\kappa(\boldsymbol{x})}\exp(-\gamma z)\left.\frac{\partial\beta}{\partial\theta}\right|_{\theta=\tilde{\theta}} \tag{49}$$

$$\overline{F}(\boldsymbol{x}, z, \tilde{\theta}) = \frac{1}{\kappa(\boldsymbol{x})}\left[\beta(\tilde{\theta}) - \tilde{\theta}\left.\frac{\partial\beta}{\partial\theta}\right|_{\theta=\tilde{\theta}}\right]\exp(-\gamma z)$$

$$+ \frac{1}{\kappa(\boldsymbol{x})}\theta(\boldsymbol{x}, 0) \tag{50}$$

The integral representation for the temperature field in the Laplace transformed domain is given by

$$\overline{\theta}(\boldsymbol{y}, p)$$

$$= \int_\Gamma \frac{\partial\overline{\theta}}{\partial n}(\boldsymbol{x}, p)\theta^*(\boldsymbol{x}, \boldsymbol{y})d\Gamma - \int_\Gamma \overline{\theta}(\boldsymbol{x}, p)\frac{\partial\theta^*}{\partial n}(\boldsymbol{x}, \boldsymbol{y})d\Gamma$$

$$- \int_\Omega \left[\frac{p}{\kappa(\boldsymbol{x})} - f_1(\boldsymbol{x}, z, \tilde{\theta})\right]\overline{\theta}(\boldsymbol{x}, p)\theta^*(\boldsymbol{x}, \boldsymbol{y})d\Omega$$

$$+ \int_\Omega \frac{k_{,i}}{k}(\boldsymbol{x})\overline{\theta}_{,i}(\boldsymbol{x}, p)\theta^*(\boldsymbol{x}, \boldsymbol{y})d\Omega$$

$$+ \int_\Omega \overline{F}(\boldsymbol{x}, z, \tilde{\theta})\theta^*(\boldsymbol{x}, \boldsymbol{y})d\Omega \tag{51}$$

where Γ is the boundary of the analyzed domain Ω and the fundamental solution is defined by $\theta^*(\boldsymbol{x}, \boldsymbol{y}) = \frac{1}{2\pi}\ln\frac{1}{r}$.

If we consider a subdomain Ω_s instead of the entire domain Ω, the following LBIE should also be valid over the subdomain

$$\begin{aligned}
&\overline{\theta}(\boldsymbol{y}, p) \\
&= \int_{\partial\Omega_s} \frac{\partial \overline{\theta}}{\partial n}(\boldsymbol{x}, p)\theta^*(\boldsymbol{x}, \boldsymbol{y})d\Gamma \\
&\quad - \int_{\partial\Omega_s} \overline{\theta}(\boldsymbol{x}, p)\frac{\partial\theta^*}{\partial n}(\boldsymbol{x}, \boldsymbol{y})d\Gamma \\
&\quad - \int_{\Omega_s} [\frac{p}{\kappa(\boldsymbol{x})} - f_1(\boldsymbol{x}, z, \tilde{\theta})]\overline{\theta}(\boldsymbol{x}, p)\theta^*(\boldsymbol{x}, \boldsymbol{y})d\Omega \\
&\quad + \int_{\Omega_s} \frac{k_{,i}}{k}(\boldsymbol{x})\overline{\theta}_{,i}(\boldsymbol{x}, p)\theta^*(\boldsymbol{x}, \boldsymbol{y})d\Omega \\
&\quad + \int_{\Omega_s} \overline{F}(\boldsymbol{x}, z, \tilde{\theta})\theta^*(\boldsymbol{x}, \boldsymbol{y})d\Omega
\end{aligned} \tag{52}$$

The integral Eq. (52) is applied to small subdomains $\Omega_s \subset \Omega$. Thus, none of the boundary densities in the Laplace transformed domain are prescribed on the local boundaries $\partial\Omega_s$ as long as they lie entirely inside Ω_s. Here again, to reduce the number of unknowns on $\partial\Omega_s$ the concept of a companion solution is utilized (Zhu *et al.*, 1998). The modified test function (7) is vanishing on the boundary of the circular subdomain of radius r_0. Since the integral Eq. (52) is also valid for the modified fundamental solution $\tilde{\theta}^*(\boldsymbol{x}, \boldsymbol{y})$, we obtain

$$\begin{aligned}
&\overline{\theta}(\boldsymbol{y}, p) \\
&= -\int_{\partial\Omega_s} \overline{\theta}(\boldsymbol{x}, p)\frac{\partial\tilde{\theta}^*}{\partial n}(\boldsymbol{x}, \boldsymbol{y})d\Gamma \\
&\quad - \int_{\Omega_s} [\frac{p}{\kappa(\boldsymbol{x})} - f_1(\boldsymbol{x}, z, \tilde{\theta})]\overline{\theta}(\boldsymbol{x}, p)\theta^*(\boldsymbol{x}, \boldsymbol{y})d\Omega \\
&\quad + \int_{\Omega_s} \frac{k_{,i}}{k}(\boldsymbol{x})\overline{\theta}_{,i}(\boldsymbol{x}, p)\tilde{\theta}^*(\boldsymbol{x}, \boldsymbol{y})d\Omega \\
&\quad + \int_{\Omega_s} \overline{F}(\boldsymbol{x}, z, \tilde{\theta})\theta^*(\boldsymbol{x}, \boldsymbol{y})d\Omega
\end{aligned} \tag{53}$$

for interior source points $\boldsymbol{y} \in \Omega$, and

$$\begin{aligned}
&\overline{\theta}(\zeta, p) \\
&= -\int_{L_s} \overline{\theta}(\boldsymbol{x}, p)\frac{\partial\tilde{\theta}^*}{\partial n}(\boldsymbol{x}, \zeta)d\Gamma \\
&\quad - \lim_{\boldsymbol{y}\to\zeta}\int_{\Gamma_s} \overline{\theta}(\boldsymbol{x}, p)\frac{\partial\tilde{\theta}^*}{\partial n}(\boldsymbol{x}, \boldsymbol{y})d\Gamma \\
&\quad + \int_{\Gamma_s} \frac{\partial \overline{\theta}}{\partial n}(\boldsymbol{x}, p)\tilde{\theta}^*(\boldsymbol{x}, \zeta)d\Gamma \\
&\quad - \int_{\Omega_s} [\frac{p}{\kappa(\boldsymbol{x})} - f_1(\boldsymbol{x}, z, \tilde{\theta})]\overline{\theta}(\boldsymbol{x}, p)\tilde{\theta}^*(\boldsymbol{x}, \zeta)d\Omega \\
&\quad + \int_{\Omega_s} \frac{k_{,i}}{k}(\boldsymbol{x})\overline{\theta}_{,i}(\boldsymbol{x}, p)\tilde{\theta}^*(\boldsymbol{x}, \zeta)d\Omega \\
&\quad + \int_{\Omega_s} \overline{F}(\boldsymbol{x}, z, \tilde{\theta})\tilde{\theta}^*(\boldsymbol{x}, \zeta)d\Omega
\end{aligned} \tag{54}$$

for source points located on the global boundary $\zeta \in \Gamma_s \subset \Gamma$. In the latter case $\partial\Omega_s = L_s \cup \Gamma_s$, where L_s is the circular part of $\partial\Omega_s$. The strongly singular integral in the integral Eq. (54) is written in the limit form.

The steady-state or stationary heat conduction equation can be obtained from the governing Eq. (46) by omitting the time-dependent term as

$$\theta_{,ii}(\boldsymbol{x}) + \frac{k_{,i}}{k}(\boldsymbol{x})\theta_{,i}(\boldsymbol{x}) = -\frac{1}{\kappa(\boldsymbol{x})}\beta(\theta)\exp(-\gamma z) \tag{55}$$

The steady-state heat conduction Eq. (55) is an elliptic partial differential equation and it is suitable for describing hot spot problems. Hot spots are localized high temperature areas caused by the temperature dependence of the thermal absorptivity. For simplicity, we assume that the thermal absorptivity is described by a power law of the form

$$\beta(\theta) = \beta_0\theta^n \tag{56}$$

According to Eq. (56), a thermal runway is possible only if $n \geq 1$ (Zhu *et al.*, 1995). Substitution of Eq. (56) into Eq. (55) leads to an eigen-value problem for the determination of the critical value of the absorptivity coefficient β_0, which can be stated as

$$\theta_{,ii}(\boldsymbol{x}) + \frac{k_{,i}}{k}(\boldsymbol{x})\theta_{,i}(\boldsymbol{x}) + \frac{1}{\kappa(\boldsymbol{x})}\beta_0[\theta(\boldsymbol{x})]^n\exp(-\gamma z) = 0 \tag{57}$$

By using the first-order Taylor-series Eq. (47), Eq. (57) can be written in a linearized form as

$$\theta_{,ii}(\boldsymbol{x}) + \frac{k_{,i}}{k}(\boldsymbol{x})\theta_{,i}(\boldsymbol{x}) + f_1(\boldsymbol{x}, z, \tilde{\theta})\theta(\boldsymbol{x}) = -F(\boldsymbol{x}, z, \tilde{\theta}) \tag{58}$$

where

$$f_i(\boldsymbol{x}, z, \tilde{\theta}) = \frac{1}{\kappa(\boldsymbol{x})}\exp(-\gamma z)\left.\frac{\partial \beta}{\partial \theta}\right|_{\theta=\tilde{\theta}}$$

$$= \frac{1}{\kappa(\boldsymbol{x})}\exp(-\gamma z)\beta_0 n\tilde{\theta}^{n-1}$$

$$F(\boldsymbol{x}, z, \tilde{\theta}) = \frac{1}{\kappa(\boldsymbol{x})}[\beta(\tilde{\theta}) - \tilde{\theta}\left.\frac{\partial \beta}{\partial \theta}\right|_{\theta=\tilde{\theta}}]\exp(-\gamma z)$$

$$= \frac{1}{\kappa(\boldsymbol{x})}\exp(-\gamma z)\beta_0(1-n)\tilde{\theta}^{n}$$

in which $\tilde{\theta}$ is the previously iterated solution for a nonlinear temperature variation of the thermal absorptivity. Note here that no iteration is needed if the coefficient n=0 and 1, i.e., when the thermal absorptivity is independent or linearly dependent on the temperature.

The solution of the eigen-value problem (58) can be given in an integral form through the LBIEs. The procedure to obtain the LBIEs is the same as in the non-stationary case. By omitting integrals representing the time-dependent term in the LBIEs (53) and (54), a system of LBIEs at interior and boundary nodes can be obtained as

$$\theta(\boldsymbol{y}) = -\int_{\partial\Omega_s}\theta(\boldsymbol{x})\frac{\partial\tilde{\theta}^*}{\partial n}(\boldsymbol{x}, \boldsymbol{y})d\Gamma + \int_{\Omega_s} f_1(\boldsymbol{x}, z, \tilde{\theta})\theta(\boldsymbol{x})\tilde{\theta}^*(\boldsymbol{x}, \boldsymbol{y})d\Omega + \int_{\Omega_s}\frac{k_{,i}}{k}(\boldsymbol{x})\theta_{,i}(\boldsymbol{x})\tilde{\theta}^*(\boldsymbol{x}, \boldsymbol{y})d\Omega + \int_{\Omega_s} F(\boldsymbol{x}, z, \tilde{\theta})\tilde{\theta}^*(\boldsymbol{x}, \boldsymbol{y})d\Omega \quad (59)$$

and

$$\theta(\zeta) = -\int_{L_s}\theta(\boldsymbol{x})\frac{\partial\tilde{\theta}^*}{\partial n}(\boldsymbol{x}, \zeta)d\Gamma - \lim_{\boldsymbol{y}\to\zeta}\int_{\Gamma_s}\theta(\boldsymbol{x})\frac{\partial\tilde{\theta}^*}{\partial n}(\boldsymbol{x}, \boldsymbol{y})d\Gamma + \int_{\Gamma_s}\frac{\partial\theta}{\partial n}(\boldsymbol{x})\tilde{\theta}^*(\boldsymbol{x}, \zeta)d\Gamma + \int_{\Omega_s} f_1(\boldsymbol{x}, z, \tilde{\theta})\theta(\boldsymbol{x})\tilde{\theta}^*(\boldsymbol{x}, \zeta)d\Omega + \int_{\Omega_s}\frac{k_{,i}}{k}(\boldsymbol{x})\theta_{,i}(\boldsymbol{x})\tilde{\theta}^*(\boldsymbol{x}, \zeta)d\Omega + \int_{\Omega_s} F(\boldsymbol{x}, z, \tilde{\theta})\tilde{\theta}^*(\boldsymbol{x}, \zeta)d\Omega \quad (60)$$

The MLS approximation is used for the numerical solution of the LBIEs. Substituting the approximation formulae (16) and (17) into the LBIEs (53) and (54) a set of linear algebraic equations is obtained as

$$\sum_{i=1}^{n}\{\phi^i(\boldsymbol{y}^b) + \int_{\partial\Omega_s}\frac{\partial\tilde{\theta}^*}{\partial n}(\boldsymbol{x}, \boldsymbol{y}^b)\phi^i(\boldsymbol{x})d\Gamma\}\hat{\theta}^i(p) = -\sum_{i=1}^{n}\int_{\Omega_s}\tilde{\theta}^*(\boldsymbol{x}, \boldsymbol{y}^b)[\frac{p}{\kappa(\boldsymbol{x})}\phi^i(\boldsymbol{x}) - f_1(\boldsymbol{x}, z, \tilde{\theta})\phi^i(\boldsymbol{x}) - \frac{k_{,j}}{k}(\boldsymbol{x})\phi^i_{,j}(\boldsymbol{x})]d\Omega\hat{\theta}^i(p) + \int_{\Omega_s}\overline{F}(\boldsymbol{x}, z, \tilde{\theta})\tilde{\theta}^*(\boldsymbol{x}, \boldsymbol{y}^b)d\Omega, \quad \text{for } \boldsymbol{y}^b\in\Omega \quad (61)$$

and

$$\sum_{i=1}^{n}\{\phi^i(\zeta^b) + \lim_{\boldsymbol{y}\to\zeta^b}\int_{\Gamma_s}\frac{\partial\tilde{\theta}^*}{\partial n}(\boldsymbol{x}, \boldsymbol{y})\phi^i(\boldsymbol{x})d\Gamma + \int_{L_s}\frac{\partial\tilde{\theta}^*}{\partial n}(\boldsymbol{x}, \zeta^b)\phi^i(\boldsymbol{x})d\Gamma - \int_{\Gamma_s} n_k\phi^i_{,k}(\boldsymbol{x})\tilde{\theta}^*(\boldsymbol{x}, \zeta^b)d\Gamma\}\hat{\theta}^i(p) = -\sum_{i=1}^{n}\int_{\Omega_s}\tilde{\theta}^*(\boldsymbol{x}, \zeta^b)[\frac{p}{\kappa(\boldsymbol{x})}\phi^i(\boldsymbol{x}) - f_1(\boldsymbol{x}, z, \tilde{\theta})\phi^i(\boldsymbol{x}) - \frac{k_{,j}}{k}(\boldsymbol{x})\phi^i_{,j}(\boldsymbol{x})]d\Omega\hat{\theta}^i(p) + \int_{\Omega_s}\overline{F}(\boldsymbol{x}, z, \tilde{\theta})\tilde{\theta}^*(\boldsymbol{x}, \zeta^b)d\Omega, \text{ for } \zeta^b\in\Gamma_{sq} \quad (62)$$

where Γ_{sq} is a part of the global boundary Γ over which the heat flux is prescribed. If the temperature is prescribed on a part $\Gamma_{s\theta}$ we collocate the approximation formula (16) by using

$$\sum_{i=1}^{n}\phi^i(\boldsymbol{x})\hat{\theta}^i(p) = \overline{\tilde{\theta}}(\zeta^b, p), \text{ for } \zeta^b\in\Gamma_{s\theta} \quad (63)$$

where $\overline{\tilde{\theta}}(\zeta^b, p)$ is the Laplace transform of the prescribed temperature.

By following essentially the same procedure, the LBIEM can be applied to steady-state or stationary microwave heating problems in FGMs. In this case, the LBIEs (59) and (60) result in a system of linear algebraic equations for the nodal values of the temperature as

Table 1 Critical β_0-values for linear thermal absorptivity in a square homogeneous plate

Decay constant	Analytical	Numerical Zhu *et al.*, 1995	Present results
γ=0	19.7	19.6	19.87
γ=2	46.4	46.0	46.7
γ=4	86.1	88.0	86.7

$$\sum_{i=1}^{n}\{\phi^i(\boldsymbol{y}^b)+\int_{\partial\Omega_s}\frac{\partial\tilde{\theta}^*}{\partial n}(\boldsymbol{x},\boldsymbol{y}^b)\phi^i(\boldsymbol{x})d\Gamma\}\hat{\theta}^i$$
$$=\sum_{i=1}^{n}\{\int_{\Omega_s}\tilde{\theta}^*(\boldsymbol{x},\boldsymbol{y}^b)[f_1(\boldsymbol{x},z,\tilde{\theta})\phi^i(\boldsymbol{x})$$
$$+\frac{k_{,j}}{k}(\boldsymbol{x})\phi^j_{,i}(\boldsymbol{x})]d\Omega\}\hat{\theta}^i$$
$$+\int_{\Omega_s}\overline{F}(\boldsymbol{x},z,\tilde{\theta})\tilde{\theta}^*(\boldsymbol{x},\boldsymbol{y}^b)d\Omega \qquad (64)$$

for $\boldsymbol{y}^b\in\Omega$, and

$$\sum_{i=1}^{n}\{\phi^i(\zeta^b)+\lim_{y\to\zeta^b}\int_{\Gamma_s}\frac{\partial\tilde{\theta}^*}{\partial n}(\boldsymbol{x},\boldsymbol{y})\phi^i(\boldsymbol{x})d\Gamma$$
$$+\int_{L_s}\frac{\partial\tilde{\theta}^*}{\partial n}(\boldsymbol{x},\zeta^b)\phi^i(\boldsymbol{x})d\Gamma$$
$$-\int_{\Gamma_s}n_k\phi^i_{,k}(\boldsymbol{x})\theta^*(\boldsymbol{x},\zeta^b)d\Gamma\}\hat{\theta}^i$$
$$=\sum_{i=1}^{n}\{\int_{\Omega_s}\tilde{\theta}^*(\boldsymbol{x},\zeta^b)[f_1(\boldsymbol{x},z,\tilde{\theta})\phi^i(x)$$
$$+\frac{k_{,j}}{k}(\boldsymbol{x})\phi^i_{,j}(\boldsymbol{x})]d\Omega\}\hat{\theta}^i$$
$$+\int_{\Omega_s}\overline{F}(\boldsymbol{x},z,\tilde{\theta})\tilde{\theta}^*(\boldsymbol{x},\zeta^b)d\Omega \qquad (65)$$

for $\zeta^b\in\Gamma_{sq}$. Also here, for prescribed temperature on $\Gamma_{s\theta}$ the following collocation formula is applied

$$\sum_{i}^{n}\phi^i(\boldsymbol{x})\hat{\theta}^i=\tilde{\theta}(\zeta^b)\text{, for }\zeta^b\in\Gamma_{s\theta} \qquad (66)$$

where $\tilde{\theta}(\zeta^b)$ is the prescribed temperature on $\zeta^b\in\Gamma_{s\theta}$.

1. Numerical Examples

(i) A Square Plate under Stationary Microwave Heating

As the first example, a square plate under a stationary microwave heating as shown in Fig. 12 is considered. On all boundaries of the square plate a uniform temperature θ=1 deg is prescribed to analyze hot spots in the plate. In our numerical calculations, a side-length a=1.0 m of the plate and a regular node distribution with 24 boundary and 23 interior nodes is used for the MLS approximation (see Fig. 12).

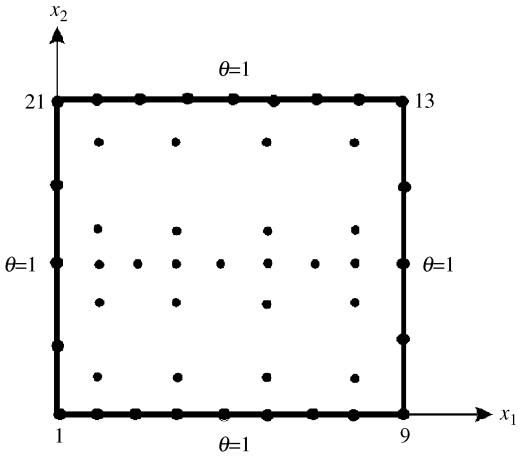

Fig. 12 Boundary conditions and node distribution for a square plate

We first consider a homogeneous plate with a linear temperature dependence of the thermal absorptivity coefficient, i.e., n=1 in Eq. (56). To obtain the critical value of the thermal absorptivity β_0 analytically, the method of Frank-Kamenetskii (1955) is used. A comparison of our numerical results with analytical and other numerical results obtained by the DRBEM (Zhu *et al.*, 1995) is given in Table 1 for three different values of the decay constant γ.

Table 1 shows a good agreement between our results and analytical and other numerical results, which demonstrates the accuracy of the LBIEM. To visualize the dependence of the temperature distribution on the parameters β_0 and γ, the steady-state temperature profiles at x_2=0.5 are presented in Fig. 13 for three values of β_0 and γ=2. It can be seen in Fig. 13 that the maximum of the temperature profile is shifted to the left side of the square plate, where a higher value of microwave energy is expected. The shift is caused by the exponential variation of the heat source in the governing Eq. (46).

Table 2 Critical β_0-values for quadratic thermal absorptivity in a square homogeneous plate

Decay constant	Analytical	TDRBEM Zhu *et al.*, 1995	LDRBEM	Present results
γ=0	4.9	4.7	4.78	4.77
γ=2	11.4	11.0	11.27	11.2
γ=4	20.1	21.0	21.09	20.3

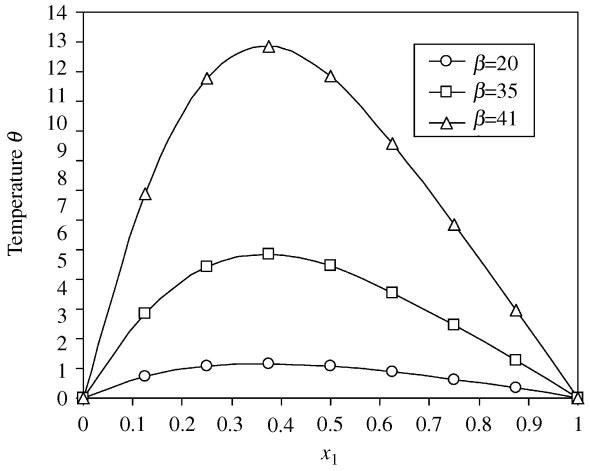

Fig. 13 Steady-state temperature profiles along x_1-axis at x_2/a= 0.5 for n=1 and γ=2

To explore the effect of the temperature dependence of the thermal absorptivity on the critical value of β_0, a homogeneous plate with a quadratic temperature dependence of the thermal absorptivity is considered in the second example, i.e., n=2 in Eq. (56). The linearized LBIEs (59) and (60) are solved by an iteration method where the first iteration value of $\tilde{\theta}$ is used as the prescribed uniform boundary quantity. The tolerance for stopping the iterations was chosen as 10^{-3}. The total number of required iterations was less than 7 in all numerical calculations. In Table 2, our numerical results are compared with analytical and other numerical results obtained by a time marching DRBEM (TDRBEM) (Zhu *et al.*, 1995) and a Laplace transform DRBEM (LDRBEM) (Zhu and Satravaha, 1996). Analytical results are obtained again by the Frank-Kamenetskii method (Frank-Kamenetskii, 1955). Table 2 shows a quite good agreement of our numerical results with analytical and other numerical results. A comparison of Table 2 with Table 1 reveals that the critical β_0-values are significantly lower for quadratic temperature dependence than for linear temperature dependence of the thermal absorptivity as given in Table 1. This means that hot spots for a quadratic temperature dependence of the thermal absorptivity occur at lower β_0-values.

Next, a square FGM plate with a spatial variation of the thermal conductivity is considered.

Table 3 Critical β_0-values for thermal absorptivity in a square FGM plate

Decay constant	Gradient parameter		
	δ=0	δ=1	δ=-1
γ=0	19.99	39.5	10.85
γ=2	46.7	86.2	25.15

Though the LBIEM presented in this paper has no restrictions on the spatial variation of the material parameters of the FGMs, an exponential variation of the material properties with Cartesian coordinates is used here. A uni-directional variation of the thermal conductivity

$$k(\boldsymbol{x})=k_0 e^{\delta x_1}$$

is applied, where k_0=1.0 $Wm^{-1}deg^{-1}$ is arbitrarily chosen. Two values of the gradient parameter δ= $\pm$1.0 m^{-1} are selected in our numerical calculations. In Table 3, the corresponding numerical results for the critical β_0-values in the FGM plate are compared with the critical β_0-values for a homogeneous plate.

One can see from Table 3 that the critical value of the absorptivity increases considerably with increasing gradient parameter for both decay constants investigated here. For a fixed gradient parameter δ, the critical value of the thermal absorptivity increases with increasing decay constant γ, which is caused by the fact that an increase of the decay constant leads to a drop of the intensity of the heat source.

For γ=0 and for two values of the gradient parameter δ, the temperature profiles at the section x_2= 0.5 are presented in Fig. 14. Fig. 14 shows that the gradient parameter δ has an influence on the temperature profile similar to the decay constant γ. For an exponential gradation of the thermal conductivity along the x_1-axis, the maximum value of the temperature is lower than the reference value corresponding to a homogeneous plate, i.e., δ=0, as shown in Fig. 14 for a fixed absorptivity parameter β_0=14.

(ii) A Square Plate under Transient Microwave Heating

The LBIEM can be also successfully applied to

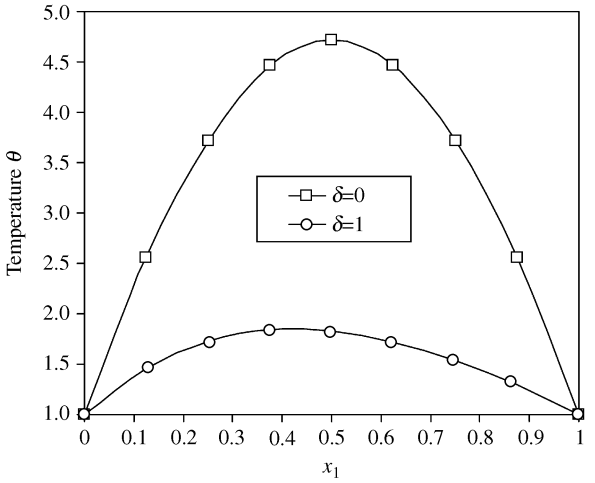

Fig. 14 Comparison of the temperature profiles in a homogeneous and an FGM square plate for β_0=14 and γ=0

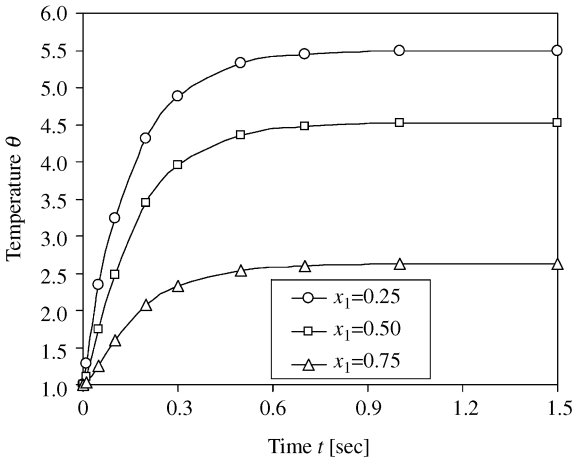

Fig. 15 Time variations of the temperature at the section x_2/a=0.5 and for β_0=64 and γ=4

transient heat conduction analysis in a solid subjected to microwave heating. To demonstrate this ability, we consider a homogeneous square plate considered in the previous example. On all sides of the square plate a thermal shock of the form $\theta(\boldsymbol{x}, t)=T\cdot H(t)$ is applied, where T=1 deg is the amplitude of the thermal shock, and $H(t)$ is the Heaviside step function. The initial condition θ=1 deg is prescribed at t=0. A linear temperature dependence of the thermal absorptivity is assumed, and Stehfest's numerical inversion method of the Laplace transform is used. The numerical results are presented in Fig. 15, which shows the time evolution of the temperature at three different positions x_1/a=0.25, 0.5, 0.75 at the middle section x_2=0.5 of the square plate for fixed values β_0=64 and γ=4. Fig. 15 shows that the temperature increases sharply with increasing time in the initial stage, and after a short time it tends to its stationary or steady-state value.

V. CONCLUSIONS

This paper summarizes recent advances in meshless LBIEM for solving heat conduction problems in continuously non-homogeneous solids such as FGMs. A reliable and efficient computational method for these materials is required due to the growing interests in FGMs for engineering applications. Heat conduction problems often occur in FGMs due to their excellent thermal properties, which are preferred for situations subjected to severe thermal loading conditions. An advanced computational method based on meshless LBIEM is presented here for 2-d, 3-d axisymmetric and microwave heating problems. Both stationary and transient heat conduction problems are dealt with. The Laplace transform and time difference techniques are applied to eliminate the time variable in the governing equations. In the time difference method the second order approximation of the time derivative is needed to obtain an accuracy comparable with that of the Laplace transform approach. The LBIEM with a meshless approximation was successfully applied to steady state and transient heat conduction analysis.

LBIEs with a simple fundamental solution vanishing on the boundary of fictitious subdomains allow the reduction of a boundary or initial-boundary value problem of continuously non-homogeneous solids into a system of linear algebraic equations with sparsely populated matrix, if a convenient domain approximation for the temperature field is used. This makes the method competitive with the FEM. Most of the available commercial computer codes based on the FEM can model the material properties only with piecewise uniform distributions within a particular element. Our meshless LBIEM puts no restrictions on material properties. The classical pure BEM formulation is restricted to special cases, where fundamental solutions for continuously non-homogeneous solids can be obtained. The conventional boundary-domain formulation is not efficient due to the coupled system of integral equations for the primary (temperature) and secondary (temperature gradients) fields with hypersingular kernels. Even in the homogeneous case when a simple fundamental solution is available, it seems to be profitable to use simplified fundamental solutions leading to boundary-domain integral formulations on small subdomains. This is advantageous, especially for elongated bodies, where the nonlocal connection between remote points in the conventional BEM leads to ill-posed algebraic systems.

Unlike the construction of interpolation functions in conventional BEM, the LBIEM with MLS approximation does not need connectivity information among points or nodes. Nodes can be randomly sprinkled in the analysed domain. It removes the well-known drawbacks of classical discretization methods associated with mesh generation. In addition, the meshless LBIEM is flexible regarding the adoption of nodal density at any location of the investigated domain, which benefits adaptive strategies to be developed in future.

The numerical implementation of the meshless LBIEM is quite easy for subdomains with a simple geometry such as circles in 2-d or spheres in 3-d. Contrary to the conventional BIEM or BEM, all integrands in the present LBIEM are regular. Hence, no special computational techniques are required to evaluate the integrals numerically. However, the complexity of the chosen shape functions in a meshless approximation may provide some difficulties in the numerical integration. By introducing small partitions in the integration domain, numerical integration errors in meshless methods can be substantially reduced. The necessity of more integration points and more complex shape functions in the meshless approach increases the computing time in comparison with conventional BIEM or BEM, where polynomial shape functions are frequently applied. Future research efforts should be directed to improving the efficiency of the meshless methods. It can be expected in the near future that the present LBIEM with an efficient meshless approximation will provide an advanced numerical tool for analyzing thermal and mechanical problems in continuously nonhomogeneous solids.

ACKNOWLEDGMENTS

The authors acknowledge the support by the Slovak Science and Technology Assistance Agency registered under number APVT-51-003702, the Slovak Grant Agency VEGA - 2303823, and the Project for Bilateral Cooperation in Science and Technology supported jointly by the International Bureau of the German BMBF and the Ministry of Education of the Slovak Republic under the project number SVK 01/020 .

REFERENCES

Atluri, S. N, Kim, H. G, and Cho, J. Y., 1999, "A Critical Assessment of the Truly Meshless Local Petrov-Galerkin (MLPG), and Local Boundary Integral Equation (LBIE) Method," *Computational Mechanics*, Vol. 24, No. 5, pp. 348-372.

Atluri, S. N., and Shen, S, 2002, *The Meshless Local Petrov-Galerkin (MLPG) Method*, Tech Science Press, Encino, CA, USA.

Atluri, S. N., Sladek, J., Sladek, V., and Zhu, T., 2000, "The Local Boundary Integral Equation (LBIE) and its Meshless Implementation for Linear Elasticity," *Computational Mechanics*, Vol. 25, Nos. 2-3, pp. 180-198.

Atluri, S. N., and Zhu, T., 1998, "A New Meshless local Petrov-Galerkin (MLPG) Approach in Computational Mechanics," *Computational Mechanics*, Vol. 22, No. 2, pp. 117-127.

Babuska, I., and Melenk, J. M., 1997, "The Partition of Unity Method," *International Journal for Numerical Methods in Engineering*, Vol. 40, No. 4, pp. 727-758.

Balas, J., Sladek, J., and Sladek, V., 1989, *Stress Analysis by Boundary Element Methods*, Elsevier, Amsterdam.

Belytschko, T., Guo, Y., Liu, W. K., and Xiao, S. P., 2000, "A Unified Stability Analysis of Meshless Particle Methods," *International Journal for Numerical Methods in Engineering*, Vol. 48, No. 9, pp. 1359-1400.

Belytschko, T., Krongauz, Y., Organ, D., Fleming, M., and Krysl, P., 1996, "Meshless Methods: An Overview and Recent Developments," *Computer Methods in Applied Mechanics and Engineering*, Vol. 139, pp. 3-47.

Belytschko, T., Lu, Y. Y., and Gu, L., 1994, "Element Free Galerkin Methods," *International Journal for Numerical Methods in Engineering*, Vol. 37, pp. 229-256.

Brebbia, C. A., Telles, J. C. F., and Wrobel, L. C., 1984, *Boundary Element Techniques*, Springer, Berlin.

Carslaw, H. S, and Jaeger, J. C., 1959, *Conduction of Heat in Solids*, Clarendon Press, Oxford, UK.

Chan, Y. S., Gray, L. J., Kaplan, T., and Paulino, G.H., 2003, "Green's Function for a Two-Dimensional Exponentially-Graded Elastic Medium," *Proceedings of the Royal Society of London A*, (in press).

Chati, M. K., and Mukherjee, S., 2000, "The Boundary Node Method for Three Dimensional Problems in Potential Theory," *International Journal for Numerical Methods in Engineering*, Vol. 47, No. 9, pp. 1523-1547.

Chati, M. K., Paulino, G. H., and Mukherjee, S., 2001, "The Meshless Standard and Hypersingular Boundary Node Methods – Applications to Error Estimation and Adaptivity in Three-Dimensional Problems," *International Journal for Numerical Methods in Engineering*, Vol. 50, No. 9, pp. 2233-2269.

Chen, J. S., Pan, C., Roque, M. O. L., and Wang, H. P., 1998, "A Lagrangian Reproducing Kernel Particle Method for Metal Forming Analysis,"

Computational Mechanics, Vol. 22, No. 3, pp. 289-307.

Ching, H. K., and Batra, R. C., 2001, "Determination of Crack Tip Fields in Linear Elastostatics by the Meshless Local Petrov-Galerkin (MLPG) Method," *CMES: Computer Modeling in Engineering and Sciences*, Vol. 2, No. 1, pp. 273-290.

Chung, H. J., and Belytschko, T., 1998, "An Error Estimate in the EFG Method," *Computational Mechanics*, Vol. 21, No. 2, pp. 91-100.

Curran, D. A., Cross, M., and Lewis, B. A., 1980, "Solution of Parabolic Differential Equations by the Boundary Element Method Using Discretization in Time," *Applied Mathematical Modelling*, Vol. 4, No. 5, pp. 398-400.

De, S., and Bathe, K .J., 2000, "The Method of Finite Spheres," *Computational Mechanics*, Vol. 25, No. 4, pp. 329-345.

Dolbow, J., and Belytschko, T., 1999, "Numerical Integration of the Galerkin Weak Form in Meshfree Methods," *Computational Mechanics*, Vol. 23, No. 3, pp. 219-230.

Duarte, C. A., and Oden, J. T., 1996, "H-p Clouds - an H-p Meshless Method," *Numerical Methods for Partial Differential Equations*, Vol. 12, No. 6, pp. 673-705.

Frank-Kamenetskii, D. A., 1955, *Diffusion and Heat Exchange in Chemical Kinetics*, Princeton University Press, Princeton.

Gavete, L., Benito, J. J., Falcon, S., and Ruiz, A., 2000, "Implementation of Essential Boundary Conditions in a Meshless Method," *Communications in Numerical Methods Engineering*, Vol. 16, No. 6, pp. 409-421.

Gray, L. J., Kaplan, T., Richardson, J. D., and Paulino, G. H., 2003, "Green's Functions and Boundary Integral Analysis for Exponentially Graded Materials: Heat Conduction," *ASME Journal of Applied Mechanics*, Vol. 70, No. 4, pp. 543-549.

Gu, Y. T., and Liu, G. R., 2001a "A Coupled Element Free Galerkin/Boundary Element Method for Stress Analysis of Two-Dimensional Solids," *Computer Methods in Applied Mechanics and Engineering*, Vol. 190, pp. 4405-4419.

Gu, Y. T., and Liu, G. R., 2001b, "A Meshless Local Petrov-Galerkin (MLPG) Formulation for Static and Free Vibration Analyses of Thin Plates," *CMES: Computer Modeling in Engineering and Sciences*, Vol. 2, No. 4, pp. 463-476.

Jin, Z. H., and Batra, R. C., 1996, "Stress Intensity Relaxation at the Tip of an Edge Crack in a Functionally Graded Material Subjected to a Thermal Shock," *Journal of Thermal Stresses*, Vol. 19, pp. 317-339.

Kaljevic, I., and Saigal, S., 1997, "An Improved Element Free Galerkin Formulation," *International Journal for Numerical Methods in Engineering*, Vol. 40, No. 16, pp. 2953-2974.

Kim, J.-H., and Paulino, G. H., 2002, "Isoparametric Graded Finite Elements for Nonhomogeneous Isotropic and Orthotropic Materials," *ASME Journal of Applied Mechanics*, Vol. 69, No. 4, pp. 502-514.

Li, S., and Liu, W. K., 1996, "Moving Least-Square Reproducing Kernel Method Part II: Fourier Analysis," *Computer Methods in Applied Mechanics and Engineering*, Vol. 139, pp. 159-193.

Liu, G. R., and Gu, Y. T., 2001, "A Point Interpolation Method for Two-Dimensional Solids," *International Journal for Numerical Methods in Engineering*, Vol. 50, No. 4, pp. 937-951.

Liu, H., and Atluri, S. N., 2000, "Meshless Local Petrov-Galerkin (MLPG) Method for Convection-Diffusion Problems," *CMES: Computer Modeling in Engineering and Sciences*, Vol. 1, No. 2, pp. 45-60.

Liu, W. K., Ade, J., and Jun, S., 1993, "Reproducing Kernel Particle Methods for Elastic and Plastic Problems," *Advanced Computational Methods for Material Modeling*, D. J. Benson and R. A., Asaro, eds., AMD 180 and PVP 33, ASME, pp. 175-190.

Liu, W. K., Li, S., and Belytschko, T., 1997, "Moving Least-Square Reproducing Kernel Methods Part I: Methodology and Convergence," *Computer Methods in Applied Mechanics and Engineering*, Vol. 143, pp. 113-154.

Martin, P. A., Richardson, J. D., Gray, L. J., and Berger, J. R., 2002, "On Green's Function for a Three-Dimensional Exponentially-Graded Elastic Solid," *Proceedings of the Royal Society of London, Series A*, Vol. 458, pp. 1931-1947.

Melenk, J. M., and Babuska, I., 1996, "The Partition of Unity Finite Element Method; Basic Theory and Applications," *Computer Methods in Applied Mechanics and Engineering*, Vol. 139, pp. 289-314.

Mikhailov, S. E., 2002, "Localized Boundary-Domain Integral Formulations for Problems with Variable Coefficients," *Engineering Analysis with Boundary Elements*, Vol. 26, No. 8, pp. 681-690.

Miyamoto, Y., Kaysser, W. A., Rabin, B. H., Kawasaki, A., and Ford, R. G., 1999, *Functionally Graded Materials: Design, Processing and Applications*, Kluwer Academic Publishers, Dordrecht.

Monaghan, J. J., 1988, "An Introduction to SPH," *Computer Physics Communications*, Vol. 48, No. 1, pp. 89- 96.

Mukherjee, Y. X., and Mukherjee, S., 1997, "Boundary Node Method for Potential Problems," *International Journal for Numerical Methods in*

En-gineering, Vol. 40, No. 5, pp. 797-815.

Mukherjee, Y. X., and Mukherjee, S., 1997, "On Boundary Conditions in the Element Free Galerkin Method," *Computational Mechanics*, Vol. 19, No. 4, pp. 264-270.

Nayroles, B., Touzot, G., and Villon, P., 1992, "Generalized FEM; Diffuse Approximation and Diffuse Elements," *Computational Mechanics*, Vol. 10, pp. 307-318.

Noda, N., and Jin, Z. H., 1993, "Thermal Stress Intensity Factors for a Crack in a Strip of a Functionally Gradient Material," *International Journal Solids and Structures*, Vol. 30, pp. 1039-1056.

Onate, E., Idelsohn, S., Zienkiewicz, O. C., and Taylor, R. L., 1996, "A Finite Point Method in Computational Mechanics; Applications to Convective Transport and Fluid Flow," *International Journal for Numerical Methods in Engineering*, Vol. 39, No. 22, pp. 3839-3866.

Ramachandran, P. A., 1990, "Application of the Boundary Element Method to Nonlinear Diffusion with Reaction Problems," *International Journal for Numerical Methods in Engineering*, Vol. 29, pp. 1021-1031.

Rizzo, F. J., and Shippy, D. J., 1970, "A Method of Solution for Certain Problems of Transient Heat Conduction," *AIAA Journal*, Vol. 8, No. 11, pp. 2004-2011.

Sladek, V., and Sladek, J., 2000, "Global and Local Integral Equations for Potential Problems in Nonhomogeneous Media," *CTU Prague Reports*, Vol. 4, pp. 133-138.

Sladek, J., Sladek, V., and Atluri, S. N., 2000b, "Local Boundary Integral Equation (LBIE) Method for Solving Problems of Elasticity with Nonhomogeneous Material Properties," *Computational Mechanics*, Vol. 24, No. 6, pp. 456-462.

Sladek, J., Sladek, V., and Atluri, S. N., 2001, "A Pure Contour Formulation for Meshless Local BoundAry Integral Equation Method in Thermoelasticity," *CMES: Computer Modeling in Engineering and Sciences*, Vol. 2, No. 4, pp. 423-434.

Sladek, V., Sladek, J., Atluri, S. N., and Van Keer, R., 2000a, "Numerical Integration of Singularities in Meshless Implementation of Local Boundary Integral Equations," *Computational Mechanics*, Vol. 25, No. 4, pp. 394-403.

Stehfest, H., 1970, "Algorithm 368: Numerical Inversion of Laplace Transform," *Communication of the Association for Computing Machinery*, Vol. 13, No. 1, pp. 47-49.

Suresh, S., and Mortensen, A., 1998, *Fundamentals of Functionally Graded Materials*, Institute of Materials, London.

Sutradhar, A., Paulino, G. H., and Gray, L. J., 2002, "Transient Heat Conduction in Homogeneous and Non-Homogeneous Materials by the Laplace Transform Galerkin Boundary Element Method," *Engineering Analysis with Boundary Elements*, Vol. 26, No. 2, pp. 119-132.

Tanaka, M., and Tanaka, K., 1980, "Transient Heat Conduction Problems in Inhomogeneous Media Discretized by Means of Boundary-Volume Element," *Nuclear Engineering and Design*, Vol. 60, No. 3, pp. 381-387.

Vignjevic, R., De Vuyst, T., and Gourna, M., 2001, "On Interpolation in SPH," *CMES: Computer Modeling in Engneering and Sciences*, Vol. 2, No. 3, pp. 319-336.

Zhu, S., Zhang, Y., and Marchant, T. R., 1995, "A DRBEM Model for Microwave Heating Problems," *Applied Mathematical Modelling*, Vol. 19, No. 5, pp. 287-297.

Zhu, S., and Satravaha, P., 1996, "An Efficient Computational Method for Modelling Transient Heat Conduction with Nonlinear Source Terms," *Applied Mathematical Modelling*, Vol. 20, No. 7, pp. 513-522.

Zhu, T., Zhang, J. D., and Atluri, S. N., 1998, "A Local Boundary Integral Equation (LBIE) Method in Computational Mechanics and Meshless Discretization Approach," *Computational Mechanics*, Vol. 21, No. 3, pp. 223-235.

Manuscript Received: Oct. 21, 2003
Revision Received: Jan. 12, 2004
and Accepted: Feb. 01, 2004